FINITE VOLUME SOLUTIONS OF 1D EULER EQUATIONS FOR HIGH SPEED FLOWS WITH FINITE-RATE CHEMISTRY

A THESIS SUBMITTED TO
THE GRADUATE SCHOOL OF NATURAL AND APPLIED SCIENCES
OF
THE MIDDLE EAST TECHNICAL UNIVERSTY

BY

BİRŞEN ERDEM

IN PARTIAL FULFILLMENT OF THE REQIREMENTS FOR THE DEGREE OF
MASTER OF SCIENCE

IN
THE DEPARTMENT OF AEROSPACE ENGINEERING

DECEMBER 2003

Approval of the Graduate School of Natural and Applied Sciences.

_____

Prof. Dr. Canan ÖZGEN

Director

I certify that this thesis satisfies all the requirements as a thesis for the degree of Master of Science.

_____

Prof. Dr. Nafiz ALEMDAROĞLU

Head of Department

This is to certify that we have read this thesis and that in our opinion it is fully adequate, in scope and quality, as a thesis for the degree of Master of Science.

_____	_____
Dr. M. Ali AK	Assoc. Prof. Dr. İsmail H. TUNCER
Co-Supervisor	Supervisor

Examining Committee Members

Prof. Dr. Nafiz ALEMDAROĞLU (Chairperson)	_____
Assoc. Prof. Dr. İsmail H. TUNCER (Supervisor)	_____
Assoc. Prof. Dr. Sinan EYİ	_____
Assist. Prof. Dr. Abdullah ULAŞ	_____
Dr. M. Ali AK (Co-Supervisor)	_____

ABSTRACT

FINITE VOLUME SOLUTIONS OF 1D EULER EQUATIONS FOR HIGH SPEED FLOWS WITH FINITE-RATE CHEMISTRY

ERDEM, Birşen

Msc., Department of Aerospace Engineering
Supervisor: Assoc. Prof. Dr. İsmail Hakkı TUNCER
Co-Supervisor: Dr. M. Ali AK

December 2003, 93 pages

In this thesis, chemically reacting flows are studied mainly for detonation problems under 1D, cylindrical and spherical symmetry conditions. The mathematical formulation of chemically reacting, inviscid, unsteady flows with species conservation equations and finite-rate chemistry is described. The Euler equations with finite-rate chemistry are discretized by Finite-Volume method and solved implicitly by using a time-spliting method. Inviscid fluxes are computed using Roe Flux Difference Splitting Model. The numerical solution is implemented in parallel using domain decomposition and PVM library routines for inter-process communication. The solution algorithm is validated first against the numerical and experimental data for a shock tube problem with and without chemical reactions and for a cylindrical and spherical propagation of a shock wave. 1D, cylindrically and spherically symmetric detonations of H_2:O_2:Ar mixture are studied next.

Keywords: Chemically Reacting Flows, Finite-Rate Chemistry, Detonation, Euler Equations.

ÖZ

YÜKSEK HIZLARDAKİ AKIŞLAR İÇİN 1 BOYUTLU EULER DENKLEMLERİNİN SONLU KİMYASAL DENKLEMLER İLE SONLU HACİMSEL ÇÖZÜMLERİ

ERDEM, Birşen

Yüksek Lisans, Uzay ve Havacılık Mühendisliği Bölümü
Tez Yöneticisi: Doç. Dr. İsmail Hakkı TUNCER
Yardımcı Tez Yöneticisi: Dr. M. Ali AK

Aralık 2003, 93 sayfa

Bu tezde, temel olarak patlama problemlerinden 1 Boyutlu (1B), silindirik ve küresel simetrik durumlar için kimyasal reaksiyonlu akışlar çalışılmıştır. Kimyasal reaksiyonlar için kütle korunumu denklemleri ile birlikte kimyasal reaksiyonlu, ağdasız, zamana bağlı akışların matematiksel ifadeleri verilmiştir. Euler denklemlerinin sonlu hızlarda gerçekleşen kimyasal reaksiyonlar ile çözümleri, sonlu hacimsel metodu kullanılarak zamanda ayrım yöntemi ile kapalı olarak çözülmüştür. Ağdasız akılar, Roe Akı Farkı Bölme modeli kullanılarak hesaplanmıştır. Sayısal çözümler, çözüm alanının küçük bölümlere ayrılması ve işlemciler arası iletişimin sağlanması için PVM kütüphanesi rutinleri kullanılarak paralel olarak elde edilmiştir. İlk olarak çözüm algoritması, şok tüp problemi, silindirik ve küresel şok dalgası yayılımı için sayısal ve deneysel veriler kullanılarak doğrulanmıştır. Daha sonra 1-B, silindirik ve küresel H_2:O_2:Ar karışımının patlaması çalışılmıştır.

Anahtar Kelimeler: Kimyasal Reaksiyonlu Akışlar, Sonlu Kimyasal Denklemler, Patlama, Euler Denklemleri.

ACKNOWLEDGMENTS

I would like to express my gratitude to my thesis supervisor Assoc. Prof. Dr. İsmail Hakkı Tuncer who guided me with his suggestions and his assistance all through my study.

I am indebted to my thesis co-supervisor and co-worker Dr. Mehmet Ali AK who had a great share in the existence of this study with his contribution.

I am thankful to Dr. Nadir SERİN for his valuable comments on different aspects of this study. Furthermore, I owe thanks to my friend Mr. Erdinç Nuri YILDIZ of his help about data processing.

I would like to acknowledge The Scientific and Technical Research Council of Turkey- Defense Industries Research and Development Institude, TÜBİTAK-SAGE for supporting the thesis work.

Lastly, I would like to express my sincere appreciation to my husband Mr. Hasan Burak ERDEM for being patient and supportive during the long and tiring thesis period. At last but not the least I would like to thank my family for listening to my compliants for all those years of my study.

TABLE OF CONTENTS

LIST OF TABLES

TABLE

LIST OF FIGURES

FIGURES

LIST OF SYMBOLS

Latin script:

a	:	Frozen speed of the sound
A	:	Pre-exponential factor
$\widetilde{A}$	:	Jacobian matrix of non-conservative variables
b	:	Temperature exponent
c	:	Speed of sound
C_i	:	Finite control volume
C_p	:	Specific heat constant of constant pressure of gas mixture
C_v	:	Specific heat constant of constant volume of gas mixture
C_{p_i}	:	Specific heat constant of constant pressure of the species
C_{v_i}	:	Specific heat constant of constant volume of the species
Da	:	Damköhler number
e	:	Internal energy of the gas mixture
e_i	:	Internal energy of the species
E_A	:	Activation energy
E	:	Total energy of the gas mixture
F	:	Conservative fluxes
$\widetilde{F}$	:	Non-conservative fluxes
$\overset{\cup}{F}$	:	Conservative flux vector
h	:	Enthalpy of the gas mixture
h_i	:	Enthalpy of the species
$h^o_{f_i}$	:	Heat of formation
I^*	:	Impulse

$k(T)$	:	Equilibrium constant
$k_{f,j}$	:	Forward reaction rate of the jth reaction
$k_{b,j}$	:	Backward reaction rate of jth reaction
K	:	Right eigenvectors of the conservative Jacobian matrices
K^{-1}	:	Left eigenvectors of the conservative Jacobian matrices
M	:	Molecular weight of the gas mixture
M_i	:	Molecular weight of the species
N	:	Right eigenvectors of the non-conservative Jacobian matrices
N^{-1}	:	Left eigenvectors of the non-conservative Jacobian matrices
N_s	:	Number of species
p	:	Pressure of the gas mixture
p_e	:	Partial derivative of pressure with respect to internal energy
p_{ρ_i}	:	Partial derivative of pressure with respect to species density
P_0	:	Atmospheric pressure
P_1	:	Pressure ahead the detonation wave
p_i	:	Partial pressure of the species
R	:	Gas constant of the gas mixture
r	:	Radial distance
R^*	:	Distance from detonation
R_i	:	Gas constant of the species
R_u	:	Universal gas constant
S	:	Conservative variable source terms
$\widetilde{S}$	:	Non-conservative variable source terms
$\overset{\cup}{S}$	:	Conservative variable source vector
T	:	Gas temperature
T'	:	Transformation matrix

u	:	Velocity of the gas mixture
U	:	Conservative variable
$\widetilde{U}$	:	Non-conservative variable
$\overset{\rho}{U}$	:	Conservative variable vector
x_i	:	Eigenvectors
X	:	Chemical formulation of 1^{st}, 2^{nd}, N^{th} species
Y_i	:	Mass fraction of reactants

Greek script:

α_i	:	Wave amplitude
β_i	:	Wave amplitude
γ	:	Specific heats of gas
$\dot{\omega}_i$	:	Source terms of the species
ρ	:	Density of the gas mixture
ρ_1	:	Density ahead the detonation wave
ρ_i	:	Density of the species
$\nu'_{i,j}$	:	Stoichiometric coefficients of reactants
$\nu''_{i,j}$	:	Stoichiometric coefficients of products
λ_i	:	Eigenvalues
σ_i	:	Slope in cell Ci
Ψ	:	Limiter

CHAPTER I

INTRODUCTION

Chemically reacting flows are becoming a significant component of modern engineering design. Chemically reacting flows are widely observed in combustion processes and hypersonic flows, for example, hypersonic reacting flows around a blunt body, rocket nozzle combustion, pre-mixed detonation, etc. Solutions of chemically reacting flows necessitate an interaction between fluid dynamics and chemical reactions among species of the fluid mixture. Euler and Navier-Stokes Equations coupled with species mass conservation equations and finite-rate chemical reactions provide the mathematical model.

I.1. Chemically Reacting Flows

Three physical processes involved in chemically reacting flows are:

- Fluid dynamics
- Thermodynamics
- Chemical reactions

The fluid dynamics process is defined by conservation of mass, momentum and energy. The thermodynamics of the reactive fluid include microscopic heat transfer between gas molecules, work done by pressure, and volume change. Chemical reactions determine the generation and/or destruction of chemical species under the constraint of mass conservation. Each of the above processes could either be evolving or in equilibrium. For the evolving condition, each process has its own space and time scales, and they may be different from that of other processes. Such differences in space and time scales could allow simplification in the theoretical model.

In this work, it is assumed that each subfield of mixture is in thermal equilibrium internally but not in equilibrium with its neighbors (local thermal equilibrium), and then equilibrium thermodynamics can be applied to each subfield. Due to the assumption of local thermal equilibrium, the concept of state variables and the equation of state in the classical thermodynamics can be used to provide the relationship between thermodynamic variables. Because of flow motion and the associated pressure and temperature distribution in the flow field, the flow field as a whole is not in thermal equilibrium. As a result, the space-time evolution of the entire non-thermally-equilibrium system can be built up by integrating the flow equations. Physically, the thermal energy of different molecules (including different species) is locally in equilibrium. Thus, there is only one temperature of the gas mixture at each space-time location [1].

In order to better understand various categories of chemically reacting flows, two time scales are defined: one associated with the fluid motion and one associated with the chemical reactions. The interaction between chemical reactions and fluid dynamics may be described by the Damköhler number [1], which is the ratio of the characteristic time of fluid mechanics to that of chemical reaction. As the Damköhler number approaches infinity, chemical reactions rates are very high for a flow and the reactions take place instantaneously. Such a flow is considered to be in equilibrium. If Damköhler number is close to zero, the chemical reactions are slow as compared to fluid flows, and it is referred as a frozen flow. In a frozen flow, fluid particles moving within the domain do not experience any change in the chemical composition. In other words, no chemical reactions take place for a frozen flow. When the Damköhler number approaches to the order of unity, a significant interaction between chemical reactions and fluid dynamics is expected. In this case, both fluid dynamics and chemical reactions should be treated as evolving processes, and one must use the finite-rate kinetics to model chemical reactions. For reacting flows, the perfect gas equation of state holds but the gas constant is temperature dependent, since the molecular weight of the mixture is changing. Chemical reactions may also cause large localized temperature variations during combustion. Therefore, it is important to accurately include the temperature dependencies in the equations of state.

Numerical solution of the Euler or Navier-Stokes Equations within species conservation terms are widely used to analyze chemically reacting flows. Chemically reacting flows which may only be investigated using finite-rate chemistry extend a simple combustion to detonation of fuel-air mixtures.

I.2. Explosion, Deflagration and Detonation

An explosion is a kind of violent, sudden and noisy reaction in which all the material changes its state from solid, liquid or gas form to hot and expanding gas. When the energy from the chemical reaction is released, pressure increases quickly. Oxidizer, flammable material and high temperature are the main three components for explosion to occur [2]. Nuclear explosions are caused by fission or fusion of atomic nuclei. In an explosion, rate of heat generation is extremely fast, but it doesn't require the passage of a combustion wave through the exploding medium.

A deflagration is a propagation of a combustion front at a velocity less than the speed of sound into the unreactant medium [3]. In other words, it is a discrete combustion wave that travels subsonically. Despite this, a deflagration can be a quite violent event.

Figure 1.1 Detonation of a high explosive

In a detonation, the propagation of combustion front has a supersonic velocity and is sustained by the energy released from the combustion [Figure 1.1], [4, 5]. High explosives which are a convenient source of extremely high-power density may detonate at standard temperature and pressure. A detonation wave can be identified as a coupled reaction zone-shock wave complex which propagates through a uniform combustible mixture to a temperature above the ignition temperature. That provides the

ignition source for the combustion to begin, and the chemical energy released in the reaction zone provides the energy required to maintain the shock wave.

Explosive events can exhibit both deflagration and detonation reactions: There is a phenomenon called the Deflagration to Detonation Transition (DDT) which describes how a deflagrating substance can detonate from released energy. In addition, reactions involving complex or multiple reactants can exhibit both due to the different reactions taking place.

Several experimental observations clarify that DDT mechanism observed on the sensitive fuel-oxygen mixtures can also be seen in fuel-air mixtures. Some experimental studies are performed to observe the transition characteristics for detonation. Mostly schlieren photographs are used to observe the sequence for the transition phenomenon as shown in Figure 1.2, [6].

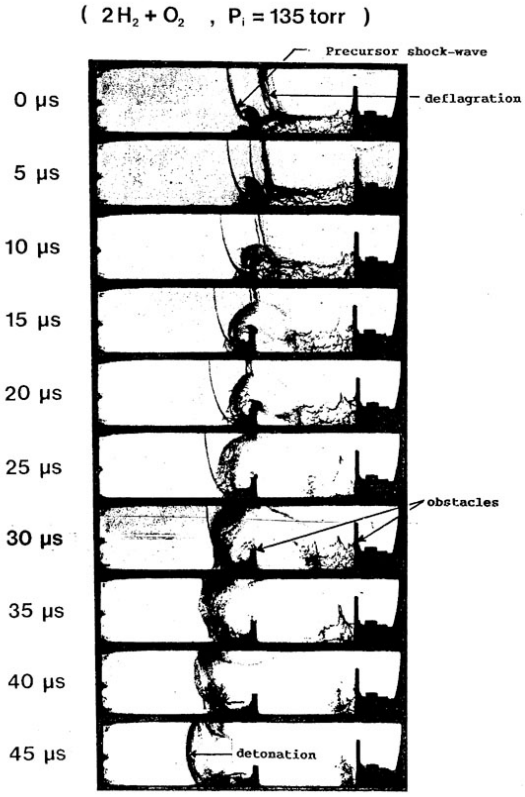

Figure 1.2 Sequence of DDT

Detonation is utilized in fuel-air explosives and pulse detonating engines. It may also occur in mines as firedamps.

I.2.1. Fuel-Air Explosives

Fuel-Air Explosives (FAE) are military weapons which are used to destroy vehicles or buildings. They are delivered by a missile, rocket or torpedo and consist of an explosive material and a detonator which is a device used to detonate the explosive. Explosives are high energy chemicals, whose energy can be released quickly by a combustion process. The combustion may be triggered by an electric spark. The oxygen required for combustion is obtained from the air. In FAE system, an aerosol cloud of fuel is first dispersed. The fuel-air mixture is ignited to produce explosion [7, 8, 9].

The detonation of the fuel is ideally performed when the fuel cloud reaches the correct diameter for the optimum stoichiometric ratio. This optimum stoichiometric ratio depicts the ratio of fuel amount to air amount required for an ideal detonation process. A first booster is used to disperse the fuel in air. After, a second booster which is projected into the cloud initiates the detonation by the shockwave effect. Note that this explosion may not be initiated by the first detonator since the fuel cloud must be detonated 0.1 to 5 seconds after the distribution of fuel into atmosphere. In Reference [10], there is a study on the measurement of the velocity of the dispersed fuel and the breaking of the droplets, their size distribution and their velocities. High speed flows in shock tubes are heavily used in the development of FAE systems.

The possible fuel list for FAE is not very large. Mostly some hydrocarbons are preferred. But also non-hydrocarbons are used. Actually the usage of hydrocarbons is highly attracted because of the accidents in the petroleum industry [11]. Some of the successfully detonated fuels are acetylene, propylene oxide, aluminum, butane, propane, and kerosene.

The shock wave produced by FAE detonation is also known as the "*blast wave*", or *"blast*". It is characterized by peak overpressure and impulse at a given distance from the center of the detonation [12, 13]. The term overpressure identifies the spectacular pressure increase due to the detonation. At some distant point from the blast origin, the passing blast wave causes the pressure to abruptly increase from the ambient

value to a large peak value, and then the pressure decays relatively slow back to the ambient value.

Effect of blast waves, *blast effectiveness*, produced by an explosion of fuel-air mixtures is a very important concern on FAE. Due to the experimental difficulties to test the blast effectiveness, the studies are mostly performed numerically, [14].

I.2.2. Pulse Detonation Engine

The other area that a detonation phenomenon is important is the pulse detonation engine (PDE). PDE is an unsteady propulsive device in which the combustion chamber is periodically filled with a reactive gas mixture, a detonation is initiated, the detonation propagates through the chamber, and the product gases are exhausted. The high pressures and resultant momentum flux out of the chamber generate thrust. Quasi-steady thrust levels can be achieved by repeating the detonation cycle at a relatively high frequency and/or using more than one combustion chamber operating out of phase as shown in Figure 1.3. Conceptually, a pulse detonation engine has some advantages when compared with the conventional propulsion systems due to its higher efficiency and higher thrust.

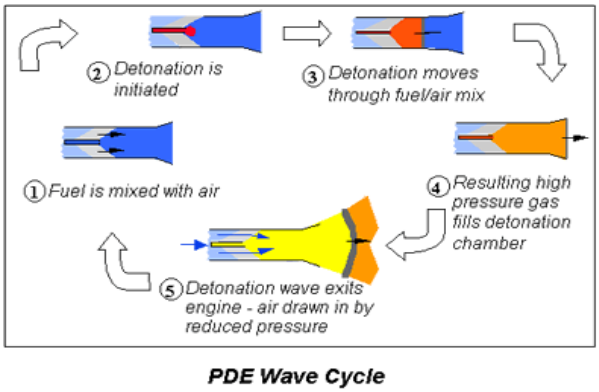

Figure 1.3 Pulse Detonation Engine Wave Cycle

Besides PDE, a pulse detonation rocket engine technology [Figure 1.4] is also being developed for boosting satellites onto higher orbits, for lunar and planetary landers and excursion vehicles that require throttle control for gentle landings. The throttle control is achieved by controlling the frequency of the detonation. Pulse

detonation rocket engines operate by injecting propellants into long cylinders that are open on one end and closed on the other.

Figure 1.4 Pulse Detonation Rocket Engine

A major advantage is that pulse detonation rocket engines boost the fuel and oxidizer to extremely high pressure without a turbo pump which is an expensive part of conventional rocket engines.

I.2.3. Firedamp or Methane Detonation

The most common industrial gases found in the mining industry are natural gas or methane (CH_4), propane (C_3H_8) and acetylene (C_2H_2) of the chemical gases. These gases originate from fossil fuels and are composed of carbon (C) and hydrogen (H). When burned, they produce carbon dioxide, water vapor and carbon monoxide. Methane is also produced when sewage or other organic matter is subject to stagnant conditions and bacterial action. Coal beds may also contain methane and release the gas when the bed is in exposed position during mining. Methane is very dangerous in underground coal mines because inadequate ventilation can result in concentrations of the gas building to explosive levels.

Since the history of mining industry, methane has been the most dangerous gas in underground mining environments. It is formed by bacterial and chemical action on organic material and it is not toxic but is particularly dangerous because it is flammable and forms an explosive mixture with air. Methane is retained within fractures, voids

and pores in rocks either as a compressed gas or adsorbed on mineral (particularly carbon) surface. Since its density is a little over half that of air, it can form pools or layers in air.

The explosible range for methane in air is normally quoted as 5% to 15%, with the most explosive mixture occurring at 9.8%. Under the normal atmosphere conditions, while the lower limit remains fairly constant, the upper explosive limit is reduced as the oxygen content of the air falls. It is also noted that the explosive limits of methane becomes a little wider as the pressure and temperature increase.

I.3. Numerical Solutions of Chemically Reacting Flows

Since 1970's, several researchers have studied the solution of chemically reacting flows using Computational Fluid Dynamics (CFD) methods. These methods, [15, 16, 17, 18, 19] are high-accuracy solution methods and especially during last years, with the improvement of the computer processing capabilities, many modern mathematical solution models have been released to open literature. However, accuracy of the CFD solution techniques strongly depends on the numerical solution algorithms used and the underlying physical sub-model. Therefore, the application of the CFD solution techniques is limited to the physical models, which can be validated experimentally.

Many modern CFD methods, originally developed for non-reactive flows, have been extended to simulate chemically reactive flows. For solving a chemically reactive flow, the first attempt is to use CFD techniques to solve the flow equations for a single component fluid with a complicated equation of state. In this approach, one can assume that the chemical reactions effect to the flow equations can be narrowed down to the space-time evolution of the molecular weight and specific heats (C_v and C_p) of the gas mixture due to the changing species composition. This situation may be represented by a complex relationship between pressure, density, and temperature, i.e., an equation of state for the reactive fluid, which is often a real gas.

Computational fluid dynamics (CFD) methods have been successfully developed and applied to calculate fluid flows under various conditions. The flow equations are usually formulated in a conservative form, and the numerical schemes are

developed to satisfy conservation of mass, momentum, and energy in a space-time domain.

Euler Equations are the conservation laws for inviscid flows. They form a first order, non-linear coupled set of equations that can be written in various forms. In reference [20], these well-known forms are conservative, non-conservative and characteristic form of the system of equations. The vectors of variables formed by density, momentum and total energy, which obey the conservation form of the equations, are called "*conservative variables"*. The direct variables such as density, pressure and velocity are called "*primitive or non-conservative variables"*. They can be measured directly in an experiment.

Numerical solution of Euler equations requires evaluation of inviscid flux terms. In finite difference and finite volume solutions, there are two different approaches to calculate inviscid fluxes at the discrete cell surface. The first approach is to use central differencing (or space-centered), where the fluxes are calculated based on the averaged flow variables at cell interfaces. Central schemes are easy to implement, but they require artificial dissipation. Another approach for the inviscid flux calculations is to use upwind schemes, which require no explicit artificial dissipation terms for stability. Currently, Upwind Schemes are preferred for their high resolution of discontinuities such as shock waves and contact discontinuities without oscillations [21].

In solution of chemically reacting flows with Euler Eqn's, viscous diffusion and heat conduction are neglected. A step that can be taken to develop accurate and efficient solutions for the eigensystems of Euler Eqn's for a flow in chemical non-equilibrium is described in reference [22].

An algorithm for flows in thermochemical non-equilibrium is described in reference [23], which presents a formulation for solving the 3D Navier-Stokes equations in generalized coordinates. This algorithm is facilitated for solution of arbitrary mixtures of thermally perfect gases in any local thermochemical state, namely full non-equilibrium, chemically non-equilibrium, chemical equilibrium or frozen flow. The thermochemical non-equilibrium flux-split schemes in three-dimensional generalized coordinates are presented, by a discussion of the time integration schemes.

Results for an axisymmetric diffusion with air and hydrogen-air chemistry, a blunt body flow, and a hydrogen-air combustion problem are supplied.

In reference [24], the Roe Flux Difference Splitting scheme is investigated for accuracy in simulating hypersonic flows. The extensions of the Roe scheme that include finite rate chemical kinetic equations follow the approach of Grossmann and Cinella. In reference [25], a procedure is proposed for the evaluation of the thermodynamic properties of air at equilibrium conditions and several generalizations of Roe's scheme are reviewed and their numerical performances are discussed by modeling 2D steady hypersonic flows.

For multicomponent flows, a new numerical scheme called Karni's Scheme is presented in [26]. This scheme is constructed to minimize the artificial oscillations that are generated by conventional finite volume schemes using Roe fluxes. A shock tube problem is solved and the results are compared with those of a classical finite volume scheme.

In reference [27], solution of thermally perfect gas flows with finite-rate chemistry by using finite difference space discreatization and TVD Runge-Kutta time discreatization with time splitting of reaction terms is presented. In reference [28], Thin Layer Navier Stokes equations for non-equilibrium hydrogen combustion are dealt with. The developed algorithm is used for blunt body, ramped duct and supersonic nozzle test cases. Also, Navier Stokes equations for chemical non-equilibrium are dealt with in reference [29]. It includes the solution of equations with Roe splitting and Van Leer splitting schemes.

A parallel CFD code which is based on Method of Lines (MOL) for transient laminar 2D reacting flows has been developed by Tarhan and Selçuk [30]. In this study, chemical reactions are modeled by infinite-rate chemistry. Governing equations are solved by MOL with high order and implicit solution algorithms. The 4^{th} order five-point Lagrange interpolation polynomial is used in spatial discreatization. The predictive ability and accuracy of the code is compared with that of other numerical studies and experimental data. Efficiencies are examined using several Ordinary Differential Equation (ODE) solvers and compared with each other. The ODE solver

ROWMAP is found the most efficient and ROWMAP ODE solver is suggested for speed and accuracy.

An experimental study on flame acceleration and transition performed with benzene-air mixtures is described in reference [31]. In this study, flame acceleration experiments are carried out in a 150 mm diameter, 3.6 m long steel tube. The entire length of the tube is filled with circular obstacles spaced one diameter apart. The fuel concentration is varied between 1.7% and 5% by volume of benzene in the fuel–air mixture. It is stated that in the experiments three regimes of propagation were observed: turbulent deflagration regime, "choking" regime and quasi-detonation regime.

In reference [32], detonation of methane/air cloud is studied by using 1D (spherically symmetric) time dependent Euler Equations with chemical kinetics. The direct initiation of methane/air cloud is modeled for different amount of an ignition source. Direct initiation means that fuel air mixture is ignited by using high explosives such as tetrly. The other mode of initiation is the self initiation. It is referred to as DDT. Finite difference approximations with Lagrangian and Eulerian features are used for conservation of mass, momentum, energy and species and also thermal and caloric equation of state with two-step oxidation mechanism. Stability of a detonation wave is also studied by W. Fishburn [33] and F.S. Hall and G.S.S. Ludfort [34].

Numerical simulations of two-dimensional laminar methane/air premixed jet flames with detailed chemical kinetics mechanism are presented in [35]. This study demonstrates the sensitivity of the modeling of detailed chemical kinetics on the flame temperature and concentrations of major component for different equivalence ratios. Numerical simulations and experimental results are in good agreement.

In another research [36], methane combustion is studied and ethane, propane and butane ignition is investigated by C.G. Fotache, H. Wang and C.K. Law [37] in counter flow of jets. For methane combustion, two-step reaction is used to analyze the interaction between different layers.

Numerical modeling of detonation is becoming a significant topic in Turkey Defense Industry. The main reason is that the research on defense industries is a confidential area and open source information on FAE warhead design is very limited.

I.4. The Scope of the Thesis

In this study, chemically reacting flows by incorporating the species conservation equations and finite-rate chemical reactions are introduced. In Chapter II, the mathematical formulations of 1D Euler Equations with finite-rate chemistry are given and non-conservative forms are presented.

In Chapter III, the flow equations are integrated in time using time-split algorithms. The numerical solutions of chemically reacting flow equations are obtained by applying the finite volume method. Flux Jacobian matrix of the system of equations, its eigenvalues and the associated eigenvector matrices are systematically derived in this chapter.

1D Euler Solver developed by M. Ali Ak [38] in 1999 is extended for chemically reacting flows. Computations are performed in parallel using domain decomposition. The developed solver is first validated with the solution of a shock tube problem with reactions in air. Next, detonation of H2:O2:Ar in a shock tube is studied to establish the accuracy of the parallel solution and the grid sensitivity of the solution algorithm. The results are compared with the numerical solution given in Reference [38]. Finally, cylindrical or spherical symmetry conditions are investigated for 3D solutions of detonation and validated by using the data given in Reference [21].

CHAPTER II

1D EULER EQUATIONS WITH FINITE-RATE CHEMISTRY

In this chapter, the mathematical formulation of inviscid, unsteady compressible flows with finite-rate chemistry is described. The mathematical equations describing inviscid flows are called Euler equations. The formulation is performed for 1D Cartesian coordinates for conservative variables. In the following part, the conservation equations for mass, momentum, energy and species are presented.

II.1. Conservation of Mass

The integral form of the law of conservation of mass by assuming no mass generation within volume, $\forall$, can be stated as:

$$\iiint_{\forall} \frac{\partial \rho}{\partial t} d\forall + \iint_{A} \vec{n}.\left(\rho \vec{V}\right) dA = 0 \qquad (2.1)$$

This integral conservation law may be generalized to include sources of mass, which will appear as additional integral terms.

Gauss Theorem is applied and Eqn. (2.1) is rewritten as:

$$\iiint_{\forall} \left[\frac{\partial \rho}{\partial t} + \nabla.\left(\rho \vec{V}\right) \right] d\forall = 0 \qquad (2.2)$$

As $\forall$ arbitrary, it follows that the integrant disappear and it becomes as,

$$\frac{\partial \rho}{\partial t} + \nabla.\left(\rho \vec{V}\right) = 0 \qquad (2.3)$$

II.2. Conservation of Momentum

The law of conservation of momentum results from the direct application of Newton's law: the time rate of change of momentum, $\rho \vec{V}$, in volume is equal to the

total force acting on the volume, $\forall$. The total force is divided into surface forces f_S and volume forces f_V.

$$\iiint_{\forall} \frac{\partial\left(\rho \vec{V}\right)}{\partial t} d\forall + \iint_{A} \vec{V}\left(n.\rho \vec{V}\right) dA = f_S + f_V \qquad (2.4)$$

Then Gauss Theorem is applied and Eqn. (2.4) is rewritten as:

$$\iiint_{\forall} \left[\frac{\partial\left(\rho \vec{V}\right)}{\partial t} + \nabla.\left[\rho \vec{V} \otimes \vec{V} + pI - \Pi\right] \right] d\forall = \iiint_{V} \rho \vec{g} d\forall \qquad (2.5)$$

As $\forall$ arbitrary, it follows that the integrant disappear,

$$\frac{\partial\left(\rho \vec{V}\right)}{\partial t} + \nabla.\left[\rho \vec{V} \otimes \vec{V} + pI - \Pi\right] = \rho \vec{g} \qquad (2.6)$$

Equation (2.6) is the differential form of momentum equation including a source term due to volume forces. When the viscous stresses are identically zero and the volume forces are neglected, Euler equations are obtained.

II.3. Conservation of Energy

The time rate of change of total energy, E_t, is equal to the work done per unit time by all the forces acting on the volume plus the influx of energy per unit time, Q, into the volume, $\forall$. The integral form of the law of conservation of energy is as follows:

$$\iiint_{\forall} \left[E_t + \nabla.\left((E + p)\vec{V} - \vec{V}.\Pi + Q\right)\right] d\forall = \iiint_{\forall} \rho\left(\vec{V}.\vec{g}\right) d\forall \qquad (2.7)$$

As V arbitrary it follows that the integrant disappear,

$$E_t + \nabla.\left[(E + p)\vec{V} - \vec{V}.\Pi + Q\right] = \rho\left(\vec{V}.\vec{g}\right) \qquad (2.8)$$

Equation (2.8) is the differential form of energy equation with the source term accounting for the effect of body forces; if these are neglected, the homogenous energy equation is obtained. When viscous and heat conduction effects are neglected, the energy equation corresponding to compressible Euler equations is obtained.

II.4. Conservation of Species

The application of the principle of conservation of mass of a species *i,* requires only a slight generalization of the development for the conservation of the total mass.

The integral form of conservation of species mass can be stated as:

$$\iiint_{\forall}\left[\frac{\partial(\rho Y_i)}{\partial t}+\nabla.\left(\rho Y_i \vec{V}\right)\right]d\forall = \iiint_{\forall} \dot{\omega}_i d\forall \tag{2.9}$$

where the density of the gas mixture can be defined as the summation of the species densities

$$\rho = \sum_{i=1}^{N_s} \rho_i \tag{2.10}$$

and Y_i, mass fraction of species i in the gas mixture can also be defined as:

$$Y_i = \frac{\rho_i}{\rho} \tag{2.11}$$

Then molecular weight of mixture is defined as follows;

$$M = \frac{1}{\sum_{i=1}^{N_s} Y_i / M_i} \tag{2.12}$$

As $\forall$ arbitrary it follows that the integrant must vanish,

$$\frac{\partial \rho_i}{\partial t}+\nabla.\left(\rho_i \vec{V}\right)= \dot{\omega}_i \tag{2.13}$$

Mass is conserved through chemical reactions and the summation of all source terms, $\dot{\omega}_i$, is zero, i.e.,

$$\sum_{i=1}^{N_s} \dot{\omega}_i = 0 \tag{2.14}$$

Thus, the summation of all species equations recovers the conservation equation of the total mass.

The source terms in the species conservation are formulated in mass concentration, and they are the summation of the rate of change of species i from all chemical reactions J:

$$\dot{\omega}_i = \frac{d\rho_i}{dt} = M_i \sum_{j=1}^{J} (\nu''_{i,j} - \nu'_{i,j})\left[(k_{f,j} \prod_{i=1}^{N_S} n_i^{\nu'_{i,j}} - k_{b,j} \prod_{i=1}^{N_S} n_i^{\nu''_{i,j}}) \right] \tag{2.15}$$

where

$$n_i = \frac{\rho_i}{M_i}$$

$\nu'_{i,j}$: Stoichiometric coefficients of reactants of i[th] species for j[th] reaction

$\nu''_{i,j}$: Stoichiometric coefficients of products of i[th] species for j[th] reaction

$k_{f,j}$: Forward reaction rate of j[th] reaction

$k_{b,j}$: Backward reaction rate of j[th] reaction

II.5. Conservative Form of 1D Euler Equations with Finite-Rate Chemistry

In this section, the detailed derivation of the 1D flow equations is presented. Conservation of species equations is incorporated with the conservation of momentum and energy equations to model chemically reacting flows. Number of species can be defined as N_s. Conservation of species equations can be added into Euler Equation in such a way that conservation of species equations, *Ns,* are written instead of global conservation of mass.

The inviscid, unsteady compressible flow equations in one spatial dimension with N_s conservation of species equations can be written as follows:

$$\frac{\partial \vec{U}}{\partial t} + \frac{\partial \vec{F}}{\partial x} = \vec{S} \tag{2.16}$$

where

$$\vec{U} = \begin{bmatrix} \rho u \\ \rho E \\ \rho_1 \\ \rho_2 \\ . \\ . \\ \rho_{N_s} \end{bmatrix} \qquad \vec{F} = \begin{bmatrix} \rho u^2 + P \\ u(\rho E + P) \\ u\,\rho_1 \\ u\rho_2 \\ . \\ . \\ u\rho_{N_s} \end{bmatrix} \qquad \vec{S} = \begin{bmatrix} 0 \\ 0 \\ \dot{\omega}_1 \\ \dot{\omega}_2 \\ . \\ . \\ \dot{\omega}_{N_s} \end{bmatrix} \tag{2.17}$$

II.6. Non-Conservative Equations

Based on the governing equations in the conservative form as shown in Eqn. (2.17) non-conservative form of the equations can be derived as in Appendix A. The

inviscid, unsteady compressible flow equations can be written in non-conservative form as follows:

$$\frac{\partial \widetilde{U}}{\partial t} + \frac{\partial \widetilde{F}}{\partial x} = \widetilde{S} \tag{2.18}$$

U is the vector of the unknown variables in the non-conservative form and is given as:

$$\widetilde{U} = \begin{pmatrix} u \\ e \\ \rho_1 \\ \rho_2 \\ \dots \\ \rho_{N_s} \end{pmatrix} \tag{2.19}$$

The governing equations in non-conservative form are given as;

Conservation of momentum equation;

$$\frac{\partial u}{\partial t} + u\frac{\partial u}{\partial x} + \frac{1}{\rho}\frac{\partial p}{\partial x} = 0 \tag{2.20}$$

Conservation of energy equation;

$$\frac{\partial e}{\partial t} + u\frac{\partial e}{\partial x} + \frac{p}{\rho}\frac{\partial u}{\partial x} = 0 \tag{2.21}$$

Conservation of mass of species equations;

$$\begin{aligned} &\frac{\partial \rho_1}{\partial t} + u\frac{\partial \rho_1}{\partial x} + \rho_1\frac{\partial u}{\partial x} = \dot{\omega}_1 \\ &\frac{\partial \rho_2}{\partial t} + u\frac{\partial \rho_2}{\partial x} + \rho_2\frac{\partial u}{\partial x} = \dot{\omega}_2 \\ &\dots \\ &\frac{\partial \rho_{N_s}}{\partial t} + u\frac{\partial \rho_{N_s}}{\partial x} + \rho_{N_s}\frac{\partial u}{\partial x} = \dot{\omega}_{N_s} \end{aligned} \tag{2.22}$$

II.6.1. Pressure

There are *Ns+2* equations and *Ns+3* unknowns including pressure for 1D Euler Equations with finite rate chemistry. An additional relation between *p* and unknown variables is needed;

$$p = p(\rho u, \rho E, \rho_1, \rho_2, \ldots, \rho_{N_s}) \tag{2.23}$$

For non-reacting flows, the calorically perfect gas equation $p=(\gamma-1)\rho e$ is used. On the other hand, a general equation of state in the form of $p=p(e, \rho_1, \rho_2, \ldots, \rho_{Ns})$ can make the flow equations (2.16) well-posed for reacting flows with the proper initial and boundary conditions [1].

First, assume that, individual species in the gas mixture behave as ideal gases,

$$P_i = \rho_i R_i T$$
where
$$R_i = \frac{R_u}{M_i} \tag{2.24}$$

where P_i and R_i are respectively the partial pressure and the gas constant of species i and $R_u=8314.34\ J/kg\text{-}moleK$ is the universal gas constant and M_i is the molecular weight of species i. Note that all species are in thermal equilibrium and they have the same temperature T.

For the model equations presented here, pressure is determined from Dalton's Law which states that the pressure of a mixture of gases is the sum of the partial pressure. Each species partial pressure is obtained from the ideal gas law as mentioned above. Thus the model equations assume a mixture of thermally perfect gases that have a pressure defined by the equation;

$$P = \sum_{i=1}^{N_s} P_i = T \sum_{i=1}^{N_s} \rho_i R_i = \rho R T \tag{2.25}$$

where

$$R = \sum_{i=1}^{N_s} Y_i R_i \tag{2.26}$$

Note that, $\partial p/\partial x$ appears in the momentum equation and p is not an unknown variable in $\tilde{U}$. Therefore, the total derivative of p can be written as follows:

$$dp = \left(\frac{\partial p}{\partial e}\right)_{\rho_j} + \sum_{i=1}^{N_s} \left(\frac{\partial p}{\partial \rho_i}\right)_{e,\rho_{j,j\neq i}} d\rho_i \tag{2.27}$$

Then,

$$p_e = \left(\frac{\partial p}{\partial e}\right)_{\rho_j}$$
$$p_{\rho_i} = \sum_{i=1}^{N_s}\left(\frac{\partial p}{\partial \rho_i}\right)_{e,\rho_{j,j\neq i}} d\rho_i \tag{2.28}$$

Taking partial derivative of p with respect to x, momentum equation is rearranged:

$$\frac{\partial p}{\partial x} = p_e \frac{\partial e}{\partial x} + \sum_{i=1}^{N_s} p_i \left(\frac{\partial \rho_i}{\partial x}\right) \tag{2.29}$$

The momentum equation in (2.20) becomes

$$\frac{\partial u}{\partial t} + u\frac{\partial u}{\partial x} + \frac{p_e}{\rho}\frac{\partial e}{\partial x} + \sum_{i=1}^{N_s}\frac{p_i}{\rho}\left(\frac{\partial \rho_i}{\partial x}\right) = 0 \tag{2.30}$$

p_e and $p_{\rho i}$ can be derived as (see Appendix B):

$$p_e = (\gamma - 1)\rho$$
$$p_{\rho_i} = \frac{R}{C_v}(e - e_i) + R_i T \tag{2.31}$$

II.6.2. Internal Energy and Enthalpy of the Mixture

The total energy E of the gas mixture is defined as;

$$E = e + \frac{u^2}{2} \tag{2.32}$$

where e is the internal energy of the gas mixture per unit mass and it is calculated based on a mass-weighted average of internal energy per unit mass of each species e_i, i.e.,

$$e = \sum_{i=1}^{N} Y_i e_i \tag{2.33}$$

The internal energy and total energy include, e_{fi}, from definitions.

The relationship between internal energy and temperature is linear for ideal gases. However, for most reacting gases, molecules can also have rotational and vibration modes in addition to translational movement. The general form of the equation for species energy in a calorically imperfect gas is given by the equation;

$$e_i = \int_{T_R}^{T} C_{vi} dT + e_{fi} \tag{2.34}$$

Then, internal energy of a gas mixture can be written as:

$$e = \int_{T_R}^{T} \sum_{i=1}^{N_s} Y_i C_{vi} dT + \sum_{i=1}^{N_s} Y_i e_{fi} = \int_{T_R}^{T} C_v dT + e_f \tag{2.35}$$

In a similar way, the general form of the equation for species enthalpy is given by the equation;

$$h_i = \int_{T_R}^{T} C_{pi} dT + h_{fi} \tag{2.36}$$

where h_{fi} is the heat of formation of species *i.*

Then, enthalpy of a gas mixture can be written as:

$$h = \int_{T_R}^{T} \sum_{i=1}^{N_s} Y_i C_{pi} dT + \sum_{i=1}^{N_s} Y_i h_{fi} = \int_{T_R}^{T} C_p dT + h_f \tag{2.37}$$

By using ideal gas equation in the definition of enthalpy h_i, Equation (2.36) can be rewritten as follows;

$$h_i = e_i + \frac{p_i}{\rho_i} = e_i + R_i T \tag{2.38}$$

$$h = \sum_{i=1}^{N_s} Y_i h_i$$

$$h = \sum_{i=1}^{N_s} Y_i e_i + \sum_{i=1}^{N_s} Y_i \frac{p_i}{\rho_i} \tag{2.39}$$

$$h = e + RT$$

II.6.3. Definition of *Cp, Cv*

C_v *and* C_P are defined as follows;

$$C_v = \left.\frac{\partial e}{dT}\right|_v = \sum_{i=1}^{N_s} Y_i C_{v_i}$$

$$C_p = \left.\frac{\partial h}{dT}\right|_p = \sum_{i=1}^{N_s} Y_i C_{p_i} \tag{2.40}$$

and the frozen specific heat ratio γ for the gas mixture is defined as;

$$\gamma = \frac{C_p}{C_v}$$

where

$$C_p = C_v + R \; ; C_p = \frac{\gamma R}{\gamma - 1} \; ; \; C_v = \frac{R}{\gamma - 1} \tag{2.41}$$

C_{pi} is not a constant, it depends on temperature and it can be obtained from measured data such as The Joint Army, Navy, NASA and Air Force tables which is called JANNAF tables [39]. In JANNAF methodology, the thermodynamic quantities, specific heat, enthalpy and entropy are evaluated at the standard atmospheric pressure ($p_0 = 1.03125x10^5\ N/m^2$). The dependence of these quantities on temperature is expressed in terms of polynomials. Several coefficients are needed for each of the three temperature ranges, 300 to 1000 K, 1000 to 6000 K and 6000 K and 20000 K. Thus, the JANNAF tables contain total 27 coefficients for each species.

$$C_{p_i} = a_{i1}T^{-2} + a_{i2}T^{-1} + a_{i3} + a_{i4}T + a_{i5}T^2 + a_{i6}T^3 + a_{i7}T^4 \tag{2.42}$$

C_v can be written as follows;

$$C_{v_i} = C_{p_i} - R_i \tag{2.43}$$

II.6.4. Temperature

The Euler equations are expressed in terms of the conserved variables; mass, momentum and energy, and do not describe temperature directly, which is determined by the internal energy of the gas. It can be obtained by substituting Eqn. (2.37), (2.26) and (2.11) into the third equation in Eqn. (2.39);

$$T = \frac{\left[\sum_{i=1}^{N_s} \frac{\rho_i}{\rho}\left(\int_{T_R}^{T} C_{P_i} dT + h_{fi}\right) - e\right]}{\frac{\sum_{i=1}^{N_s} \rho_i R_i}{\rho}} \tag{2.44}$$

II.7. Finite-Rate Chemistry

In a general mixture of *Ns* species there will be *J* reactions taking place;

$$\nu'_{1,j}X_1 + \nu'_{1,j}X_2 + ... + \nu'_{1,j}X_N \leftrightarrow \nu''_{1,j}X_1 + \nu''_{1,j}X_2 + ... + \nu''_{1,j}X_N \qquad \text{j} = 1,2, \ \ ,\text{J} \quad (2.45)$$

X : Chemical formulation of 1st, 2nd, Nth species

Generally the forward and backward reaction rates are determined empirically and tabulated through the use of curve fits. The most common curve fit used for chemistry reaction rates is the Arrhenius equation. Although tabulation of experimental values for rate coeffients in Arhenius form is common, current practice frequently utilized the three parameter functional form:

$$k(T) = AT^b \exp(-E_A / R_u T) \qquad (2.46)$$

where *A, b,* and E_A are the three empirical parameters which can be obtained from the CHEMKIN databases [40].

II.8. Additional Terms in the Euler Equations Due to Cylindrical and Spherical Symmetry

Cylindrical and spherical symmetric wave motion arises naturally in the theory of explosion wave in water, air and other media. In these situations the multi dimensional equations may be reduced to essentially 1D equations with a geometric source term *S(U)* to account for 2nd and 3rd spatial dimensions. Then the Euler equation without species conservation equations becomes as [21]:

$$\frac{\partial U}{\partial t} + \frac{\partial F(U)_r}{\partial x} = S(U)$$

where (2.47)

$$U = \begin{bmatrix} \rho \\ \rho u \\ \rho E \end{bmatrix} \qquad F = \begin{bmatrix} \rho u \\ \rho u^2 + P \\ u(\rho E + P) \end{bmatrix} \qquad \text{S} = -\frac{\alpha}{r}\begin{bmatrix} \rho u \\ \rho u^2 \\ u(\rho E + p) \end{bmatrix}$$

If we add the above source terms in Eqn. (2.12), the unsteady, inviscid, and chemically reacting flow equations in one spatial dimension become as;

$$U = \begin{bmatrix} \rho u \\ \rho E \\ \rho_1 \\ \rho_2 \\ . \\ . \\ \rho_{N_s} \end{bmatrix} \qquad F = \begin{bmatrix} \rho u^2 + P \\ u(\rho E + P) \\ u\,\rho_1 \\ u\rho_2 \\ . \\ . \\ u\rho_{N_s} \end{bmatrix} \qquad S = \begin{bmatrix} -\frac{\alpha}{r}\rho u^2 \\ -\frac{\alpha}{r}u(\rho E + P) \\ \dot{\omega}_1 - \frac{\alpha}{r}\rho_1 u \\ \dot{\omega}_2 - \frac{\alpha}{r}\rho_2 u \\ . \\ . \\ \dot{\omega}_{N_s} - \frac{\alpha}{r}\rho_{N_s} u \end{bmatrix} \tag{2.48}$$

The cylindrical (when α=1) and spherical (when α=2) symmetry approximation may also be solved numerically by the current 1D solution method with a minor modification.

CHAPTER III

NUMERICAL SOLUTION OF GOVERNING EQUATIONS

In the previous chapter, 1D Euler equations with Finite-Rate Chemistry are given in both conservative form and non-conservative form. Due to numerical difficulties in the solution of conservative form of Euler equations, non-conservative form of these equations is employed in the numerical solution. The non-conservative form of the system of equations can also be given in a vector form as follows (See Chapter II):

$$\frac{\partial \widetilde{U}}{\partial t} + \frac{\partial \widetilde{F}}{\partial x} = \widetilde{S} \tag{3.1}$$

Equation (3.1) can be solved in two ways: fully coupled or loosely coupled by splitting the equations into homogenous and non-homogenous part. The splitting becomes;

$$\left.\begin{aligned} PDE &: \frac{\partial \overset{\rho}{U}}{\partial t} + \frac{\partial \overset{\rho}{F}}{\partial x} = 0 \\ IC &: U(x, t^n) = \overset{\rho}{U}^n \end{aligned}\right\} \overline{U}^{n+1} \tag{3.2}$$

$$\left.\begin{aligned} ODE &: \frac{d\overset{\rho}{U}}{dt} = \overset{\rho}{S} \\ IC &: \overline{U}^{n+1} \end{aligned}\right\} \overset{\rho}{U}^{n+1} \tag{3.3}$$

Finite Volume Method (FVM) is used to solve the homogenous part and an ODE solver is used to solve the non-homogenous part. Finite volume space and time discreatization are given first. Finally, an ODE solver named DLSODE using to solve

source terms that come from chemistry and spherical symmetry mentioned in Chapter II is mentioned.

Eqn. (3.2) can be expressed in different form as follows:

$$\frac{\partial \widetilde{U}}{\partial t} + \frac{\partial \widetilde{F}}{\partial \widetilde{U}} \frac{\partial \widetilde{U}}{\partial x} = 0 \tag{3.4}$$

$$\widetilde{A} = \frac{\partial \widetilde{F}}{\partial \widetilde{U}}$$
$$\frac{\partial \widetilde{U}}{\partial t} + \widetilde{A} \frac{\partial \widetilde{U}}{\partial x} = 0 \tag{3.5}$$

where $\tilde{A}$ is called as Jacobian Matrix of System of Equations.

The time dependent Euler equations are hyperbolic equations, i.e., if the Jacobian matrix of flux function has *m* real and distinct eigenvalues and a corresponding set of *m* linearly independent eigenvectors, the system is said to be strictly hyperbolic where *m* is the total number of equations of the system. Therefore, Jacobian Matrix and its eigenvalues and eigenvectors are found to solve these system of equations. The eigenvalues of the matrix $\tilde{A}$ are obtained from the determinant of the following;

$$\left| \widetilde{A} - \lambda I \right| = 0 \tag{3.6}$$

The flux evaluation is the most important step in this solution. Flux modeling plays an important role in accurate and physically valid solution. In the next section, the Riemann problem and Godunov Flux is reviewed first. Roe Flux Difference Splitting Method is then introduced. In the second part, the ODE solver, DLSODE, is introduced.

III.1. Flux Modeling

For better understanding of flux modeling, Riemann problem and Godunov Method should be mentioned firstly. After that, Roe Flux Difference Splitting Method is described in the following subsections and Roe Fluxes for 1D Euler Equations with Finite Rate Chemistry are formulated.

III.1.1. Riemann Problem

The Riemann problem can be identified for the hyperbolic, constant coefficient system:

$$PDE: \quad U_t + AU_x = 0$$
$$ICs: \quad U(x,0) = U^0(x) = \begin{cases} U_L & x < 0, \\ U_R & x > 0 \end{cases} \tag{3.7}$$

The structure of the the solution of the Riemann problem in *x-t* plane is given in Figure 3.1. For *mxm* linear hyperbolic system, it consists of *m* waves coming from origin.

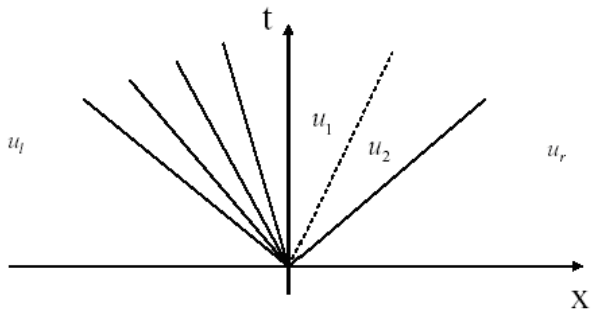

Figure 3.1 Structure of the Solution of the Riemann Problem for a general linear hyperbolic system

Each wave carries a jump discontinuity in *U,* propagating with speed λ_i. The solution of the left side of the waves is simply the initial data U_L and the solution of the right side is U_R. The task is to find the solution between wedge of waves. As the eigenvectors $K^{(1)}$, $K^{(2)}$,..., $K^{(m)}$ are linearly independent, U_L and U_R can be written as follows:

$$U_L = \sum_{i=1}^{m} \alpha_i K^{(i)}, \; U_R = \sum_{i=1}^{m} \beta_i K^{(i)} \tag{3.8}$$

where α_i and β_i are constant coefficients for $i=1,...,m$. For a given point (x,t) there is an eigen value λ_I such that $\lambda_I < x/t < \lambda_{I+1}$., that is $x-\lambda_i t>0$ such that $i \leq I$. Then the final solution of the Riemann problem can be written as:

$$U(x,t) = \sum_{i=1+1}^{m} \alpha_i K^{(i)} + \sum_{i=1}^{I} \beta_i K^{(i)} \tag{3.9}$$

Physically, Riemann problem is a slight generalization of the shock-tube problem. In this problem, the aim is to find the fluxes between left and right wedge of waves in *x-t* plane called as star region which is the region between left and right state. For 1D Euler Equations, a solution method can be found at Chapter 4 in [21].

III.1.2. Godunov Method

Godunov's scheme utilize Approximate Riemann solvers. To understand the Godunov Method, firstly 1D non-linear hyperbolic system of Initial-Boundary Value Problem (IVBP) should be considered;

$$\left.\begin{array}{ll} PDE: & U_t + F(U_x) = o \\ ICs: & U(x,0) = U^0(x) \\ BCs: & \\ & \left.\begin{array}{l} U(0,t) = U_L \\ U(L,t) = U_R \end{array}\right\} \end{array}\right\} \qquad (3.10)$$

Godunov method assumes a piece-wise constant distribution of the data as seen in Figure 3.2.

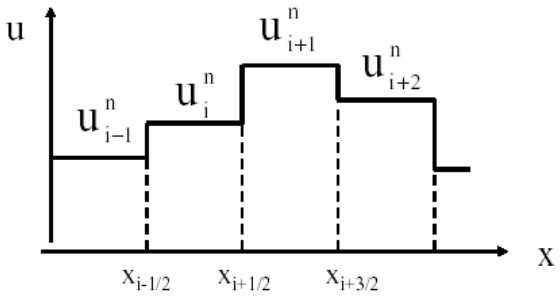

Figure 3.2 Piece-wise constant distribution of data at time level n

Spatial discretization of finite volumes is denoted as $x_i = x_{i-1} + \Delta x$ and temporal discretization is given as $t^{n+1} = t^n + \Delta t$.

Cell averages are defined as:

$$U_i^n = \frac{1}{\Delta x} \int_{x_{i-1/2}}^{x_{i+1/2}} \tilde{U}(x, t^n) dx \qquad (3.11)$$

and they produce the desired piecewise constant distribution $U(x,t^n)$, with U^i for x in each cell $[x_{i-1/2}, x_{i+1/2}]$.

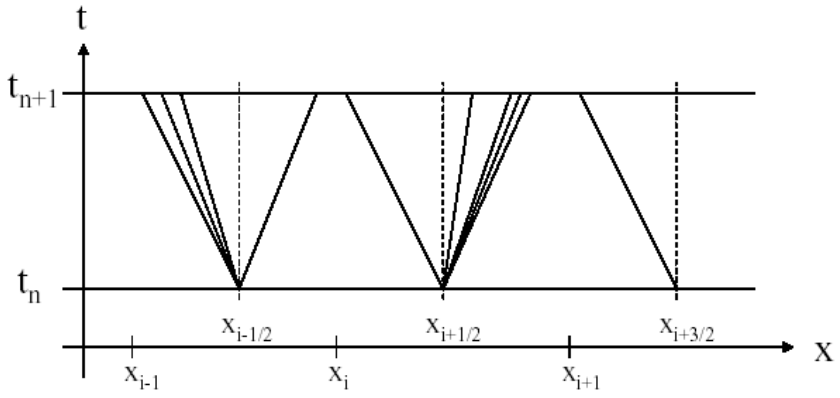

Figure 3.3 Typical wave patterns of local Riemann problems at intercell boundaries *i-1/2* and *i+1/2*

Figure 3.3 shows typical wave patterns emanating from the intercell boundaries $x_{i-1/2}$ and $x_{i+1/2}$ when solving the Riemann problems of (U_{i-1}, U_i) and(U_i, U_{i+1}). For a time step, Δt, that is small enough to avoid wave interaction, a global solution in terms of local solutions can be obtained and Godunov method can be written in conservative form:

$$U_i^{n+1} = U_i^n + \frac{\Delta t}{\Delta x}\left[F_{i-1/2} + F_{i+1/2}\right] \tag{3.12}$$

with intercell numerical flux given by

$$F_{i+1/2} = F\left(U_{i+1/2}(0)\right) \tag{3.13}$$

and details on Godunov Method can be found in [20].

Roe Flux Difference Splitting (FDS) Method based on Godunov Method is one of the upwind methods mentioned in Chapter I. In this study, the flux at the interface of control volumes is modeled by Roe's scheme.

III.1.3. Roe Flux Differencing Method

Roe Flux Differencing Method is used to solve fluxes in Equation (3.2) and it is examined in this section. Equation (3.2) can be written in terms of Jacobian Matrix as follows:

$$\left.\begin{aligned} &PDE: \quad U_t + AU_x = o \\ &U(x,0) = \begin{cases} U_L, & x < 0 \\ U_R, & x > 0 \end{cases} \end{aligned}\right\} \tag{3.14}$$

Roe's approach replaces the Jacobian matrix by a constant Jacobian matrix

$$\overline{A} = \overline{A}(U_L, U_R) \tag{3.15}$$

Therefore, the original problem is replaced by

$$U_t + \overline{A}U_x = 0 \tag{3.16}$$

The original Riemann problem is then replaced by the approximate Riemann problem.

$$\left.\begin{aligned} &PDE: \quad U_t + \overline{A}U_x = o \\ &U(x,0) = \begin{cases} U_L, & x < 0 \\ U_R, & x > 0 \end{cases} \end{aligned}\right\} \tag{3.17}$$

This Roe Jacobian matrix satisfies the following properties;

1- It has linearly independent eigenvalues,

2- It is consistent with the exact Jacobian,

3- It conserves the discontinuities.

The eigenvalues and the right eigenvectors of the matrix $\overline{A}(U_L, U_R)$ are as follows respectively;

$$\begin{aligned} &\overline{\lambda}_i(U_L, U_R) \\ &\overline{K}^{(i)}(U_L, U_R) \end{aligned} \tag{3.18}$$

The intercell fluxes are calculated in the following procedure:

$$\begin{aligned} &\Delta U = U_R - U_L = \sum_{i=1}^{n} \overline{\alpha}_i \overline{K}^{(i)} \\ &\overline{\alpha}_i = \overline{\alpha}_i(U_L, U_R), \text{ wave strenght} \end{aligned} \tag{3.19}$$

$$U_{i+1/2}(0) = U_L + \sum_{\tilde{\lambda}_i \le 0} \overline{\alpha}_i \overline{K}^{(i)}$$

or (3.20)

$$U_{i+1/2}(0) = U_R - \sum_{\tilde{\lambda}_i \ge 0} \overline{\alpha}_i \overline{K}^{(i)}$$

Now, the corresponding numerical flux is found from modified system of conservation laws,

$$\overline{U}_t + \overline{F}\left(\overline{U}\right)_x = o \tag{3.21}$$

where flux function is written as:

$$\begin{aligned} \overline{F}\left(\overline{U}\right) &= \overline{A}\,\overline{U} \\ F_{i+1/2} &= \overline{A}\,\overline{U}_{i+1/2}(0) \end{aligned} \tag{3.22}$$

Finally, using Eqn. (3.35) the numerical fluxes are obtained from

$$F_{i+1/2} = F_L + \sum_{\tilde{\lambda}_i \le 0} \overline{\alpha}_i \overline{\lambda}_i \overline{K}^{(i)}$$

or (3.23)

$$F_{i+1/2} = F_R - \sum_{\tilde{\lambda}_i \ge 0} \overline{\alpha}_i \overline{\lambda}_i \overline{K}^{(i)}$$

Alternatively, it can be written,

$$F_{i+1/2} = \frac{1}{2}\left(F_L + F_R\right) - \frac{1}{2}\sum_{i=0}^{m} \overline{\alpha}_i \left|\overline{\lambda}_i\right| \overline{K}^{(i)} \tag{3.24}$$

In order to compute Roe fluxes for a particular system of conservation laws, the wave strenghts α_i, and the eigenvalues λ_i and the right eigenvectors $K^{(i)}$ can be obtained from the Jacobian matrix $\tilde{A}$ of the non-conservative form of the system of equations. The calculation of Roe fluxes for 1D Euler Equations with Finite-Rate Chemistry can be obtained using wave strenghts α_i, and eigenvalues λ_i and the right eigenvectors $K^{(i)}$ of the Jacobian matrix $\tilde{A}$ of the non-conservative form of the system of equations in the following subsection.

III.1.4. Roe Fluxes for 1D Euler Equations with Finite Rate Chemistry

To solve Roe fluxes, Jacobian matrix of the non-conservative system of equations can be required and it is also given by [1] as follows;

$$\widetilde{A} = \begin{bmatrix} u & p_e/\rho & p_{\rho_1}/\rho & p_{\rho_2}/\rho & \dots & p_{\rho_{N_s}}/\rho \\ p/\rho & u & 0 & 0 & \dots & 0 \\ \rho_1 & 0 & u & 0 & \dots & 0 \\ \rho_2 & 0 & 0 & u & \dots & 0 \\ \dots & \dots & \dots & \dots & \dots & \dots \\ \rho_{N_s} & 0 & 0 & 0 & \dots & u \end{bmatrix} \tag{3.25}$$

Eigenvalues of the matrix $\tilde{A}$ are obtained from the determinant of the following;

$$\left|\widetilde{A} - \widetilde{\lambda} I\right| = 0 \tag{3.26}$$

where I is the identity matrix. Due to simplicity of the non-conservative form equations, the $Ns+2$ eigenvalues of $\tilde{A}$ are found to be;

$$\begin{aligned} \widetilde{\lambda}_i &= u + \sqrt{\gamma RT} \\ &= u - \sqrt{\gamma RT} \\ &= u \end{aligned} \tag{3.27}$$

where $a = \sqrt{\gamma RT}$ is the frozen speed of sound of the gas mixture.

The right eigenvector x_i of the matrix $\tilde{A}$ associated with the eigenvalue λ_i can be obtained by solving;

$$\widetilde{A} x_i = \widetilde{\lambda}_i x_i \tag{3.28}$$

to get nontrivial solution for x_i of the Jacobian matrix. The related eigenvectors of $u \pm a$, u eigenvalues can be found by using a Symbolic Math Software.

$$\begin{bmatrix} 1 \\ p/a\rho \\ \rho_1/a \\ \rho_2/a \\ \dots \\ \rho_{N_s}/a \end{bmatrix} \begin{bmatrix} 1 \\ -p/a\rho \\ -\rho_1/a \\ -\rho_2/a \\ \dots \\ -\rho_{Ns}/a \end{bmatrix} \begin{bmatrix} 0 \\ 1 \\ -p_e/p_{\rho_1} \\ 0 \\ \dots \\ 0 \end{bmatrix} \begin{bmatrix} 0 \\ 1 \\ 0 \\ -p_e/p_{\rho_1} \\ \dots \\ 0 \end{bmatrix} \dots\dots \begin{bmatrix} 0 \\ 0 \\ 1 \\ 0 \\ \dots \\ -p_e/p_{\rho_{N_s}} \end{bmatrix} \tag{3.29}$$

Thus, we get the Right and Left Eigenvectors of the non-conservative form of the system of Euler equations with chemical reacting flows. The Right Eigenvector Matrix, N is given as follows (The Left Eigenvector Matrix N^{-1} is given in Appendix C):

$$N=\begin{bmatrix} 1 & 1 & 0 & 0 & 0 \\ p/a\rho & -p/a\rho & 1 & 1 & 0 \\ \rho_1/a & -\rho_1/a & -p_e/p_{\rho_1} & 0 & 1 \\ \rho_2/a & -\rho_2/a & 0 & -p_e/p_{\rho_1} \quad ..... & 0 \\ ... & ... & ... & ... & ... \\ \rho_{Ns}/a & -\rho_{Ns}/a & 0 & 0 & -p_e/p_{\rho_{Ns}} \end{bmatrix} \tag{3.30}$$

Now, the non-conservative equations must be transformed to conservative equations by multiplying it with transformation matrix T^t and The Right Eigenvectors of Jacobian matrix of the conservative equations can also be found by the following multiplication:

$$K = T^t N \tag{3.31}$$

Right Eigenvector of Jacobian matrix of the conservative equations is given as follows and Left Eigenvector Matrix K^{-1} is given in Appendix C:

$$K=\begin{bmatrix} \rho\left(1+\frac{u}{a}\right) & \rho\left(1-\frac{u}{a}\right) & -u\frac{P_e}{P_{\rho_1}} & ... & -u\frac{P_e}{P_{\rho_{Ns}}} \\ \rho\left(u+\frac{E}{a}\right)+\frac{P}{a} & \rho\left(u-\frac{E}{a}\right)-\frac{P}{a} & \rho-E\frac{P_e}{P_{\rho_1}} & ... & \rho-E\frac{P_e}{P_{\rho_{Ns}}} \\ \frac{\rho_1}{a} & -\frac{\rho_1}{a} & -\frac{P_e}{P_{\rho_1}} & ... & 0 \\ ... & ... & ... & ... & ... \\ \frac{\rho_{Ns}}{a} & -\frac{\rho_{Ns}}{a} & 0 & ... & -\frac{P_e}{P_{\rho_{Ns}}} \end{bmatrix} \tag{3.32}$$

Roe Averaged Values are defined as (see [41]);

$$\hat{\rho} = \sqrt{\rho_L \rho_R} \tag{3.33}$$

$$\hat{u} = \frac{\sqrt{\rho_L}u_L + \sqrt{\rho_R}u_R}{\sqrt{\rho_L} + \sqrt{\rho_R}} \tag{3.34}$$

$$\hat{E} = \frac{\sqrt{\rho_L}E_L + \sqrt{\rho_R}E_R}{\sqrt{\rho_L} + \sqrt{\rho_R}} \tag{3.35}$$

$$\hat{H} = \frac{\sqrt{\rho_L}H_L + \sqrt{\rho_R}H_R}{\sqrt{\rho_L} + \sqrt{\rho_R}} \tag{3.36}$$

$$\hat{\rho}_i = \frac{\sqrt{\rho_L}\rho_{iL} + \sqrt{\rho_R}\rho_{iR}}{\sqrt{\rho_L} + \sqrt{\rho_R}} \tag{3.37}$$

$$\hat{Y}_i = \frac{\sqrt{\rho_L}Y_{iL} + \sqrt{\rho_R}Y_{iR}}{\sqrt{\rho_L} + \sqrt{\rho_R}} \tag{3.38}$$

$$\hat{e}_i = \frac{\sqrt{\rho_L}e_{iL} + \sqrt{\rho_R}e_{iR}}{\sqrt{\rho_L} + \sqrt{\rho_R}} \tag{3.39}$$

$$\hat{T} = \frac{\sqrt{\rho_L}T_L + \sqrt{\rho_R}T_R}{\sqrt{\rho_L} + \sqrt{\rho_R}} \tag{3.40}$$

$$\hat{R} = \sum_{i=1}^{N} \hat{Y}_i R_i \tag{3.41}$$

$$\hat{c}_v = \sum_{i=1}^{N} \hat{Y}_i \overline{c}_{vi} \tag{3.42}$$

$$\overline{c}_{vi} = \frac{1}{T_R - T_L}\int_{T_L}^{T_R} c_{vi}dT \tag{3.43}$$

$$\hat{\gamma} - 1 = \frac{\hat{R}}{\hat{c}_v} \tag{3.44}$$

$$a^2 = (\hat{\gamma} - 1)\left(\hat{H} - \frac{\hat{u}^2}{2} + \hat{c}_v\hat{T} - \sum_{i=1}^{N}\hat{Y}_i\hat{e}_i\right) \tag{3.45}$$

$$\hat{P}_e = (\hat{\gamma} - 1)\hat{\rho} \tag{3.46}$$

By introducing Roe averaged variables, Eigenvector matrix becomes as follows:

$$\hat{K} = \begin{bmatrix} \hat{\rho}\left(1 + \frac{\hat{u}}{\hat{a}}\right) & \hat{\rho}\left(1 - \frac{\hat{u}}{a}\right) & -\hat{u}\frac{\hat{P}_e}{\hat{P}_{\rho_1}} & \dots & -\hat{u}\frac{\hat{P}_e}{\hat{P}_{\rho_{Ns}}} \\ \frac{\hat{\rho}}{\hat{a}}\left(\hat{H} + \hat{u}\hat{a}\right) & \frac{\hat{\rho}}{\hat{a}}\left(\hat{u}\hat{a} - \hat{H}\right) & \hat{\rho} - \hat{E}\frac{\hat{P}_e}{\hat{P}_{\rho_1}} & \dots & \hat{\rho} - \hat{E}\frac{\hat{P}_e}{\hat{P}_{\rho_{Ns}}} \\ \frac{\hat{\rho}_1}{\hat{a}} & -\frac{\hat{\rho}_1}{\hat{a}} & -\frac{\hat{P}_e}{\hat{P}_{\rho_1}} & \dots & 0 \\ \dots & \dots & \dots & \dots & \dots \\ \frac{\hat{\rho}_{Ns}}{\hat{a}} & -\frac{\hat{\rho}_2}{\hat{a}} & 0 & \dots & -\frac{\hat{P}_e}{\hat{P}_{\rho_{Ns}}} \end{bmatrix} \tag{3.47}$$

1D Right Eigenvector Matrix for Jacobian matrix can be written for only 2 species to derive the wave strenghts given in Eqn. (3.24),

$$K = \begin{bmatrix} \rho\left(1+\frac{u}{a}\right) & \rho\left(1-\frac{u}{a}\right) & -u\frac{P_e}{P_{\rho_1}} & -u\frac{P_e}{P_{\rho 2}} \\ \rho\left(u+\frac{E}{a}\right)+\frac{P}{a} & \rho\left(u-\frac{E}{a}\right)-\frac{P}{a} & \rho - E\frac{P_e}{P_{\rho_1}} & \rho - E\frac{P_e}{P_{\rho_2}} \\ \frac{\rho_1}{a} & -\frac{\rho_1}{a} & -\frac{P_e}{P_{\rho_2}} & 0 \\ \frac{\rho_2}{a} & -\frac{\rho_2}{a} & 0 & -\frac{P_e}{P_{\rho_2}} \end{bmatrix} \tag{3.48}$$

Then 1D wave strengths vector can be taken as;

$$\alpha = \begin{bmatrix} \alpha_1 \\ \alpha_2 \\ \alpha_3 \\ \alpha_4 \end{bmatrix} \tag{3.49}$$

and the 1D conservative jump in the variable vector can be defined as;

$$\Delta u = \begin{bmatrix} \Delta u_1 \\ \Delta u_2 \\ \Delta u_3 \\ \Delta u_4 \end{bmatrix} \tag{3.50}$$

The relation between 1D conservative variable jump vector and characteristics can be written as:

$$K \cdot \alpha = \Delta u \tag{3.51}$$

1D wave strengths require solution of the following linear system which is given in compact form in Eqn. (3.43),

$$\begin{bmatrix} \rho\left(1+\frac{u}{a}\right) & \rho\left(1-\frac{u}{a}\right) & -u\frac{P_e}{P_{\rho_1}} & -u\frac{P_e}{P_{\rho 2}} \\ \rho\left(u+\frac{E}{a}\right)+\frac{P}{a} & \rho\left(u-\frac{E}{a}\right)-\frac{P}{a} & \rho - E\frac{P_e}{P_{\rho_1}} & \rho - E\frac{P_e}{P_{\rho_2}} \\ \frac{\rho_1}{a} & -\frac{\rho_1}{a} & -\frac{P_e}{P_{\rho_2}} & 0 \\ \frac{\rho_2}{a} & -\frac{\rho_2}{a} & 0 & -\frac{P_e}{P_{\rho_2}} \end{bmatrix} \cdot \begin{bmatrix} \alpha_1 \\ \alpha_2 \\ \alpha_3 \\ \alpha_4 \end{bmatrix} = \begin{bmatrix} \Delta u_1 \\ \Delta u_2 \\ \Delta u_3 \\ \Delta u_4 \end{bmatrix} \tag{3.52}$$

from 3th and 4th equations of the matrix multiplication,

$$\alpha_1 \frac{\rho_1}{a} - \alpha_2 \frac{\rho_1}{a} - \alpha_3 \frac{P_e}{P_{\rho_1}} = \Delta u_3 \tag{3.53}$$

$$\alpha_1 \frac{\rho_2}{a} - \alpha_2 \frac{\rho_2}{a} - \alpha_4 \frac{P_e}{P_{\rho_2}} = \Delta u_4 \tag{3.54}$$

Adding (3.53) and (3.54),

$$\alpha_1 \frac{\rho}{a} - \alpha_2 \frac{\rho}{a} - \alpha_3 \frac{P_e}{P_{\rho_1}} - \alpha_4 \frac{P_e}{P_{\rho_2}} = \Delta u_3 + \Delta u_4 \tag{3.55}$$

From 1st equation of the matrix multiplication;

$$\rho\left(1+\frac{u}{a}\right)\alpha_1 + \rho\left(1-\frac{u}{a}\right)\alpha_2 - u\frac{P_e}{P_{\rho_1}}\alpha_3 - u\frac{P_e}{P_{\rho_2}}\alpha_4 = \Delta u_1 \tag{3.56}$$

$$\rho\alpha_1 + \rho\alpha_2 + u\left(\frac{\rho}{a}\alpha_1 - \frac{\rho}{a}\alpha_2 - \frac{P_e}{P_{\rho_1}}\alpha_3 - \frac{P_e}{P_{\rho_2}}\alpha_4\right) = \Delta u_1 \tag{3.57}$$

By using Eqn. (3.55), Eqn. (3.53) becomes

$$\rho\alpha_1 + \rho\alpha_2 + u\left(\Delta u_3 + \Delta u_4\right) = \Delta u_1 \tag{3.58}$$

$$\alpha_1 + \alpha_2 = \frac{1}{\rho}\left\{\Delta u_1 - u\left(\Delta u_3 + \Delta u_4\right)\right\} \tag{3.59}$$

From 2nd equation of the matrix multiplication;

$$\left\{\rho\left(u+\frac{E}{a}\right)+\frac{P}{a}\right\}\alpha_1 + \left\{\rho\left(u-\frac{E}{a}\right)-\frac{P}{a}\right\}\alpha_2 + \left(\rho - E\frac{P_e}{P_{\rho_1}}\right)\alpha_3 + \left(\rho - E\frac{P_e}{P_{\rho_2}}\right)\alpha_4 = \Delta u_2 \tag{3.60}$$

$$\left(\rho u + \frac{P}{a}\right)\alpha_1 + \left(\rho u - \frac{P}{a}\right)\alpha_2 + \rho\alpha_3 + \rho\alpha_4 + E\left(\frac{\rho}{a}\alpha_1 - \frac{\rho}{a}\alpha_2 - \frac{P_e}{P_{\rho_1}}\alpha_3 - \frac{P_e}{P_{\rho_2}}\alpha_4\right) = \Delta u_2 \tag{3.61}$$

By using Eqn. (3.55), Eqn. (3.54) becomes

$$\left(\rho u + \frac{P}{a}\right)\alpha_1 + \left(\rho u - \frac{P}{a}\right)\alpha_2 + \rho\alpha_3 + \rho\alpha_4 + E\left(\Delta u_3 + \Delta u_4\right) = \Delta u_2 \tag{3.62}$$

$$\left(\rho u + \frac{P}{a}\right)\alpha_1 + \left(\rho u - \frac{P}{a}\right)\alpha_2 + \rho\alpha_3 + \rho\alpha_4 = \Delta u_2 - E\left(\Delta u_3 + \Delta u_4\right) \tag{3.63}$$

From Eqn. (3.53) 3rd wave strength is found to be

$$\alpha_3 = \frac{P_{\rho_1}}{P_e}\left(\frac{\rho_1}{a}\alpha_1 - \frac{\rho_1}{a}\alpha_2 - \Delta u_3\right) \tag{3.64}$$

Similarly from Equation (3.54) 4th wave strength is found to be

$$\alpha_4 = \frac{P_{\rho_2}}{P_e}\left(\frac{\rho_2}{a}\alpha_1 - \frac{\rho_2}{a}\alpha_2 - \Delta u_4\right) \tag{3.65}$$

Inserting (3.64) and (3.65) to (3.63),

$$\begin{aligned}&\left(\rho u + \frac{P}{a}\right)\alpha_1 + \left(\rho u - \frac{P}{a}\right)\alpha_2 + \rho\frac{P_{\rho_1}}{P_e}\left(\frac{\rho_1}{a}\alpha_1 - \frac{\rho_1}{a}\alpha_2 - \Delta u_3\right)\\ &+ \rho\frac{P_{\rho_2}}{P_e}\left(\frac{\rho_2}{a}\alpha_1 - \frac{\rho_2}{a}\alpha_2 - \Delta u_4\right) = \Delta u_2 - E\left(\Delta u_3 + \Delta u_4\right)\end{aligned} \tag{3.66}$$

$$\begin{aligned}&\left(\rho u + \frac{P}{a} + \frac{\rho}{a}\sum_{i=1}^{2}\frac{\rho_i P_{\rho_i}}{P_e}\right)\alpha_1 + \left(\rho u - \frac{P}{a} - \frac{\rho}{a}\sum_{i=1}^{2}\frac{\rho_i P_{\rho_i}}{P_e}\right)\alpha_2\\ &= \Delta u_2 - E\left(\Delta u_3 + \Delta u_4\right) + \rho\frac{P_{\rho_1}}{P_e}\Delta u_3 + \rho\frac{P_{\rho_2}}{P_e}\Delta u_4\end{aligned} \tag{3.67}$$

Finally, written in compact form for *N* species

$$\begin{aligned}&\left(\rho u + \frac{P}{a} + \frac{\rho}{a}\sum_{i=1}^{N}\frac{\rho_i P_{\rho_i}}{P_e}\right)\alpha_1 + \left(\rho u - \frac{P}{a} - \frac{\rho}{a}\sum_{i=1}^{N}\frac{\rho_i P_{\rho_i}}{P_e}\right)\alpha_2\\ &= \Delta u_2 - E\sum_{i=1}^{N}\Delta u_{2+i} + \sum_{i=1}^{N}\rho\frac{P_{\rho_i}}{P_e}\Delta u_{2+i}\end{aligned} \tag{3.68}$$

from the definition of static enthalpy

$$h = \frac{P}{\rho} + \sum_{i=1}^{N}\frac{\rho_i P_{\rho_i}}{P_e} = C_p T \tag{3.69}$$

$$\frac{\rho}{a}\left(h + ua\right)\alpha_1 + \frac{\rho}{a}\left(-h + ua\right)\alpha_2 = \Delta u_2 - E\sum_{i=1}^{N}\Delta u_{2+i} + \sum_{i=1}^{N}\rho\frac{P_{\rho_i}}{P_e}\Delta u_{2+i} \tag{3.70}$$

$$\left(h + ua\right)\alpha_1 + \left(-h + ua\right)\alpha_2 = \frac{a}{\rho}\Delta u_2 - \frac{a}{\rho}E\sum_{i=1}^{N}\Delta u_{2+i} + a\sum_{i=1}^{N}\frac{P_{\rho_i}}{P_e}\Delta u_{2+i} = RHS1 \tag{3.71}$$

Multiplying (3.59) with $\left(h + ua\right)$

$$\left(h + ua\right)\alpha_1 + \left(h + ua\right)\alpha_2 = \frac{h + ua}{\rho}\left\{\Delta u_1 - u\left(\Delta u_3 + \Delta u_4\right)\right\} = RHS2 \tag{3.72}$$

and subtracting from (3.71), second wave strength is found to be

$$\alpha_2 = \frac{1}{2h}\left(RHS2 - RHS1\right) \tag{3.73}$$

Finally first wave strength is found to be

$$\alpha_1 = \frac{1}{\rho}\left\{\Delta u_1 - u\left(\Delta u_3 + \Delta u_4\right)\right\} - \alpha_2 \tag{3.74}$$

For *N* species, wave strengths are the following:

$$\alpha_2 = \frac{1}{2h}\left(RHS2 - RHS1\right) \tag{3.75}$$

$$\alpha_1 = \frac{1}{\rho}\left\{\Delta u_1 - u\sum_{i=1}^{N}\Delta u_{2+i}\right\} - \alpha_2 \tag{3.76}$$

$$\alpha_{2+i} = \frac{P_{\rho_i}}{P_e}\left(\frac{\rho_i}{a}\alpha_1 - \frac{\rho_i}{a}\alpha_2 - \Delta u_{2+i}\right) \tag{3.77}$$

III.2. 1D inviscid, compressible (Euler) solver

1D, 2D, 3D Euler flow solvers with Roe fluxes was developed by Ak [38] in 1999. In this study, 1D Euler solver is extended for the solution of chemically reacting flows by finite-rate chemistry. 1D inviscid, compressible (Euler) solver has a main program which is called Euler 1D and sixteen subroutines and algorithm of the solver will be given in detail below. There are two major part of 1D inviscid, compressible (Euler) solver. One of the major part executes the flux calculations and the second part computes the source terms of species conservation equations and additional source terms of momentum, energy equations coming from spherical symmetry.

Roe flux solver is implemented in a subroutine named as *FLUX*. Wave strenghts and Roe averaged values of fluxes given in subsection III.1.4 are computed in this subroutine. The Roe fluxes evaluated at the cell interface are modified by a Slope Limiter.

The limited slope within the cell is calculated by introducing the slope limiter as follows:

$$\sigma_i = \frac{w_{i+1}^n - w_i^n}{\delta x}\Psi_i \tag{3.78}$$

where Ψ_i is the non-linear limiting function of cell C_i and fluxes at the intercell are defined as:

$$F_{i+1/2} = F_L + \sum_{\tilde{\lambda}_i \le 0} \alpha_i \lambda_i K^i + \frac{1}{2} \sum_{\tilde{\lambda}_i \le 0} |\lambda_i| \left[1 - \frac{dt|\lambda_i|}{\delta x} \right] \alpha_i K^i \Psi_i \tag{3.79}$$

$$\Psi(r) = \max[0, \min(2r, l), \min(r, 2)] \tag{3.80}$$

where r is the ratio of slopes of cell *i-1, i, i+1*.The detail on the second order accurate flux calculation can be found from [21], [38].

The ODE solver is implemented in a subroutine named as *ODE* which calculates source terms that come from conservation of species mass and spherical symmetry. It sets up the proper variables and calls *DLSODE* which is the Ordinary Differential Equation (ODE) solver.

For a detonation wave, there are serious difficulties in designing numerical methods which properly account for the fluid dynamics and the chemistry. For sufficient fine meshes such difficulties can be overcome but cost will be very high. Because of that, ODE solver which is planned to be used must be chosen very carefully. In this study, Double precision Livermore Solver for Ordinary Differential Equations named *DLSODE* is implemented. It is one of the stiff ODE solvers for solving source terms coming from conservation of species mass and spherical symmetry in the Euler Equations with finite-rate chemistry. *DLSODE* solves stiff and non-stiff systems of the form *dy/dt = f (t, y)*. In the stiff case, it treats the Jacobian matrix *df/dy* either as a dense (full) matrix, or as user-supplied or internally approximated by difference quotients. It uses Adams methods (predictor-corrector) in the non-stiff case and Backward Differentiation Formula (BDF) methods (the Gear methods) in the stiff case. The linear systems are solved by direct methods. Documentation on the usage of DLSODE is provided from the open literature.

Also time discretization is very important for this problem, because time scales of flow and chemical reactions are far away from each other, therefore time step must be calculated from time scales of either chemical reactions or flow. Time discretization is re-built from *cfl* number called Courant Friderich Lewis number.

In 1D inviscid, compressible (Euler) solver, conservative variables are computed using subroutine *ODE* for first half of *dt* then by using these conservative variables, fluxes are re-calculated from subroutine *FLUX* for each time step. Finally, conservative variables are calculated from subroutine *ODE* for the last half of *dt*.

III.2.1. Parallel Computation of 1D inviscid, compressible (Euler) solver

Parallel computing is the concept of executing a program on multiprocessors by diving a large problem into smaller parts. By allocating the *n* processors, it is expected that the same program run *n* times faster than with a single processor [30, 42]. In this study, domain decomposition method is used for parallel implementation. 1D domain is partitioned into n subdomains with two cell overlapping at the subdomain boundaries. Solution on each subdomain is assigned to a parallel computer. Inter domain boundary conditions are exchanged at every five step of the unsteady solution. Parallel virtual machine (PVM) message passing software is used for the information exchange between sub-domains. In parallel computing, performance can be defined by speed-up and efficiency. Speed-up is the ratio of the execution times of parallel and single computing. Efficieny is the ratio of speed-up to number of processors.

1D inviscid, compressible (Euler) solver is also developed for parallel computing and algorithm of it is given in Figure 3.4. Additional subroutines are written for master and worker processors called subroutine *MAIN* and subroutine *WORKER*. Parallel computations are are done using the processors in the Parallel Computing Laboratory of TÜBİTAK-SAGE, i.e. The Scientific and Technical Research Council of Turkey/ Defence Industry Research and Development Institude. Parallel computing for 1D inviscid, compressible (Euler) solver is executed using two or higher processors whose speed-up information is given in the next chapter.

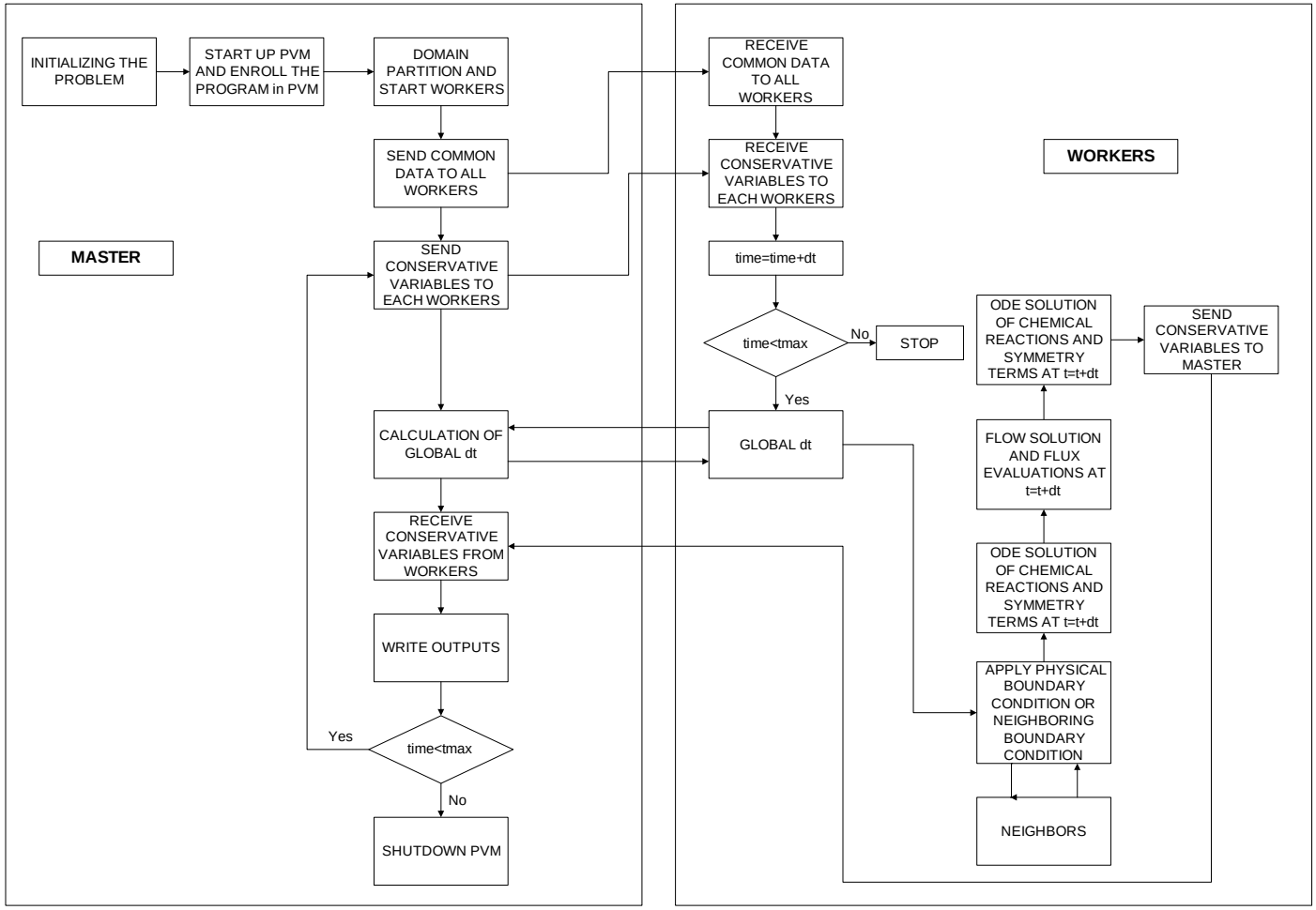

Figure 3.4 Algorithm of 1D inviscid, compressible (Euler) solver with Finite-Rate Chemistry

CHAPTER IV

RESULTS AND DISCUSSIONS

In this chapter, the Euler solver developed for the solution of 1D inviscid, compressible flows with species conservation of mass equations and finite-rate chemistry is first validated by the solution of a shock tube problem for air by comparing the original Euler solver developed earlier by Ak [38]. Numerical solutions are also compared with the exact solutions in [20].

Next, a 1D detonation of H_2:O_2:Ar mixture at high temperature is studied. The results with chemical reactions are validated against the numerical data given in Reference [43]. Parallel solutions are also validated against the serial solution and a grid refinement study is performed.

An axis-symmetric (cylindrical symmetry) and spherical symmetry detonation cases are computed as a third test case and it is validated where the source terms for cylindrical and spherical symmetry terms are activated against the numerical data given in Reference [21].

Finally, the detonation of H_2:O_2:Ar given in Reference [44] is also studied under cylindrical and spherical symmetry conditions. The results obtained are compared with each other and are validated by against the numerical data. The results for both cylindrical and spherical symmetry cases are also compared with the linear detonation solution.

IV.1. Validation of 1D Euler Solver: Shock (Sode) Tube Problem

The shock tube problem forms a particularly difficult test problem since it represents an exact solution to the full system of 1D Euler Equations containing simultaneously, a shock wave, a contact discontinuity and an expansion fan. This problem can be realized experimentally by sudden breakdown of a diaphragm in a long

1D tube separating two initial gas states at different pressures and densities as shown in Figure 4.1.

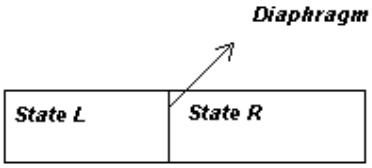

Figure 4.1 Sode Tube with Initial State at t=0

The initial pressures and densities for this particular case are 10^5 Pa and 1 kg/m^3 at the left side and 10^4 Pa with 0.125 kg/m^3 at the right hand side of the tube. Symmetry boundary conditions are applied in the calculations at x=0 and x=10 m as a wall boundary condition. The computed solutions with the present solver and the original 1D Euler solver are given in Figure 4.2. Shock wave and contact discontinuity are detected without any oscillation. The numerical results compare well with the results given in Reference [38].

Table 4.1 Reaction Mechanisms for Air

Reactions	**A $(m^3mol^{-1})^{r-1}s^{-1}$**	**b**	**$E_A(Jmol^{-1})$**
O2+M=>2O+M	2.90E+23	-2.0	59750.
N2+M=>2N+M	1.60E+22	-1.6	113200.
NO+M=>N+O+M	7.95E+23	-2.0	75500.
NO+O=>N+O2	8.37E+12	0.0	19450.
O+N2=>N+NO	6.44E+17	-1.0	38370.

For the same case given above, the solution with the present solver where species conservation of mass and chemical reaction taken place, are obtained. Both solution and the exact solutions given in Reference [20] are compared in Figure 4.2. In this figure, distribution of mass fraction of O_2 and N_2 are given only for present solver.

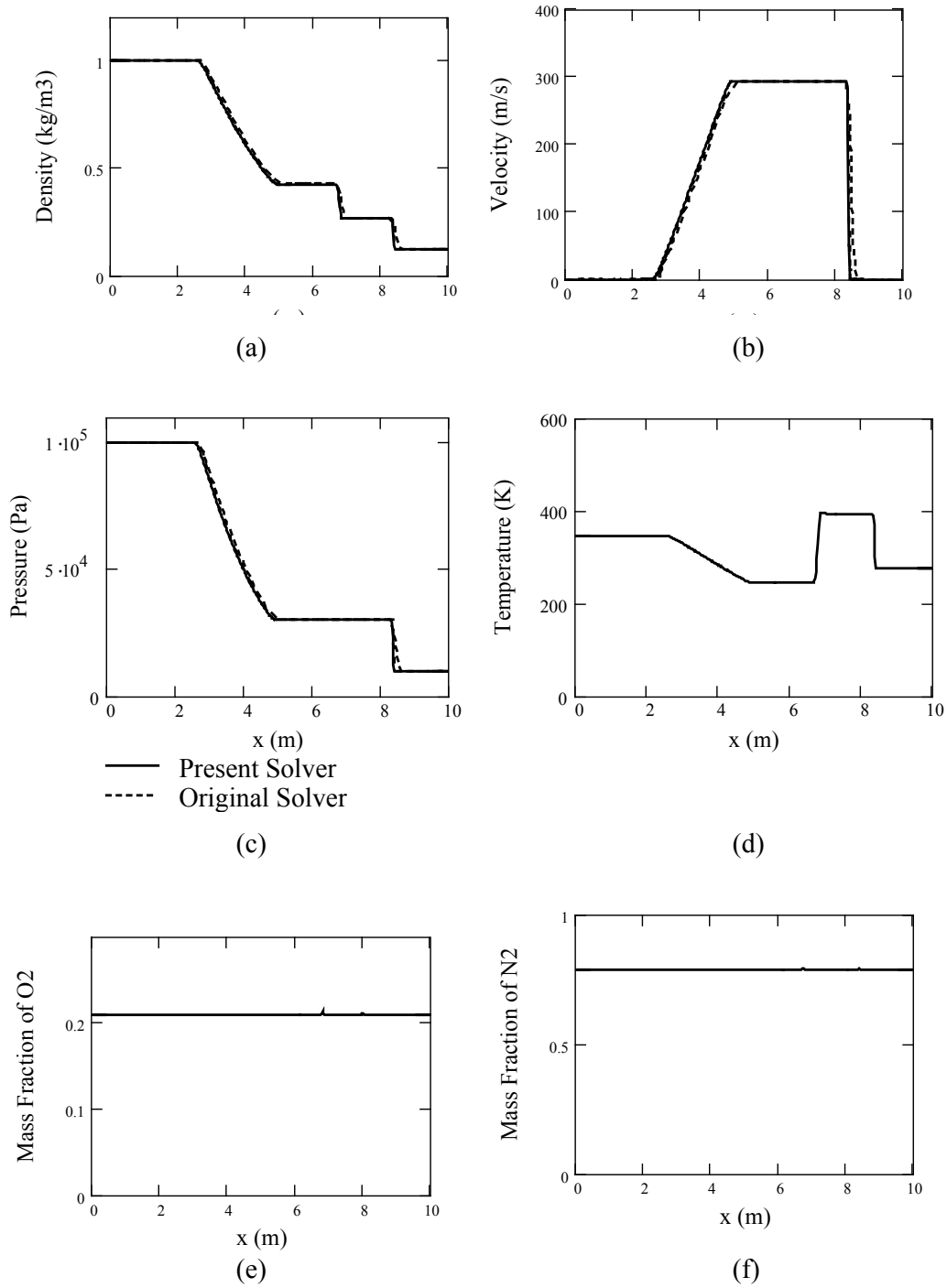

Figure 4.2 Distribution of density (a), velocity (b), pressure (c), temperature (d) and mass fraction of O_2 (e) and N_2 (f) in a shock tube at 6.1 msec

IV.2. Detonation of H_2:O_2:Ar in a Shock Tube

In this case, the shock tube is assumed to filled with a H_2:O_2:Ar mixture of molar ratios 2:1:7. The tube, which is closed at one end, is 12 cm long. As an initial condition, an incident shock wave traveling from open end on the right to the wall on the left is given. The computations start at instant the shock hits the wall. When the shock wave hits the wall boundary on the left, it is immediately reflected and a new shock wave travels to the right. Initial states of this problem are given in Reference [43] as [see Table 4.2].

Table 4.2 Initial Data for Shock Tube with Non-Equilibrium Chemistry

Variables	**Incident Shock**	**Reflected Shock**
ρ [kg/m^3]	0.223128	0.4889
u [m/s]	-478.5	0.0
P [Pa]	36679.65	131820
T [K]	624	1036
Y_{H2}:Y_{O2}:Y_{Ar}	0.012773 : 0.101369 : 0.885858	
W [kg/mol]	3.156667 10^{-2}	

This particular 1D example has been studied in the past and a well validated reaction mechanism for numerical simulations is available in different references. It utilizes 9 different chemical species; O_2, H_2O, H, O, OH, H_2, HO_2, H_2O_2 and Ar and 48 non-equilibrium elementary reactions given in Table 4.3 [43].

The unsteady flow with the initial conditions given above is computed by the present solver in serial and in parallel. The results are compared to each other in Figure 4.3. As shown the solutions obtained in parallel overlap with the serial solution. It is concluded that the accuracy of the computations is preserved. However, the efficiency of parallel computations degrades gradually as the number of processors increase due to loss during inter-process communication. The speed-up which is the execution times ratio between parallel and single solver is collected and shown in Figure 4.4. In the same figure, efficiency, the slope of this curve, is also seen.

Table 4.3 Reaction Mechanisms of H_2:O_2:Ar

Reactions	**A((kg/mol)$^{n-1}$s) b**	**E_A(J/mol)**
H + OH => O + H2	0.843E+10 1.00	6955.
O + H2 => H + OH	0.181E+11 1.00	8903.
H + HO2 => H2 + O2	0.253E+14 0.00	696.
H2 + O2 => H + HO2	0.548E+14 0.00	57828.
H + HO2 => OH + OH	0.253E+15 0.00	1888.
OH + OH => H + HO2	0.120E+14 0.00	40142.
H + HO2 => O + H2O	0.500E+14 0.00	994.
O + H2O => H + HO2	0.105E+13 0.45	56437.
H + H2O2 => HO2 + H2	0.169E+13 0.00	3776.
HO2 + H2 => H + H2O2	0.723E+12 0.00	18680.
H + H2O2 => OH + H2O	0.318E+15 0.00	8943.
OH + H2O => H + H2O2	0.240E+15 0.00	80483.
OH + H2 => H + H2O	0.110E+10 1.30	3657.
H + H2O => OH + H2	0.108E+11 1.20	19097.
OH + OH => H2 + O2	0.656E+11 0.26	29212.
H2 + O2 => OH + OH	0.169E+14 0.00	48091.
OH + OH => O + H2O	0.602E+08 1.30	0.
O + H2O => OH + OH	0.193E+10 1.16	17428.
OH + HO2 => H2O + O2	0.500E+14 0.00	1000.
H2O + O2 => OH + HO2	0.143E+15 0.17	73329.
OH + H2O2 => HO2 + H2O	0.102E+14 0.00	1808.
HO2 + H2O => OH + H2O2	0.283E+14 0.00	32789.
HO2 + H2 => OH + H2O	0.723E+12 0.00	18700.
OH + H2O => HO2 + H2	0.801E+10 0.43	71938.
HO2 + HO2 => H2O2 + O2	0.181E+14 0.00	994.
H2O2 + O2 => HO2 + HO2	0.945E+15 -0.38	43719.
O + OH => H + O2	0.164E+13 0.28	-161.
H + O2 => O + OH	0.223E+15 0.00	16792.
O + HO2 => OH + O2	0.501E+14 0.00	1000.
OH + O2 => O + HO2	0.132E+14 0.18	56040.
O + H2O2 => H2O + O2	0.843E+12 0.00	4213.
H2O + O2 => O + H2O2	0.343E+11 0.52	89028.
O + H2O2 => OH + HO2	0.843E+12 0.00	4233.
OH + HO2 => O + H2O2	0.125E+10 0.64	16355.
H2 + M => H + H + M	0.223E+15 0.00	95983.
H2O + M => H + OH + M	0.349E+16 0.00	105124.
HO2 + M => H + O2 + M	0.211E+16 0.00	45706.
H2O2 + M => OH + OH + M	0.120E+18 0.00	45508.
OH + M => O + H + M	0.140E+15 0.21	101349.
HO2 + M => O + OH + M	0.662E+20 -0.43	63989.
O2 + M => O + O + M	0.181E+19 -1.00	118041.
H + H +M => H2 + M	0.653E+18 -1.00	0.
H + OH+M => H2O + M	0.225E+23 -2.00	0.
H + O2 +M => HO2 + M	0.150E+16 0.00	-994.
OH + OH+M => H2O2 + M	0.907E+15 0.00	-5067.
O + H +M => OH + M	0.300E+20 -1.00	0.
O + OH+M => HO2 + M	0.102E+18 0.00	0.
O + O +M => O2 + M	0.189E+14 0.00	-1789.

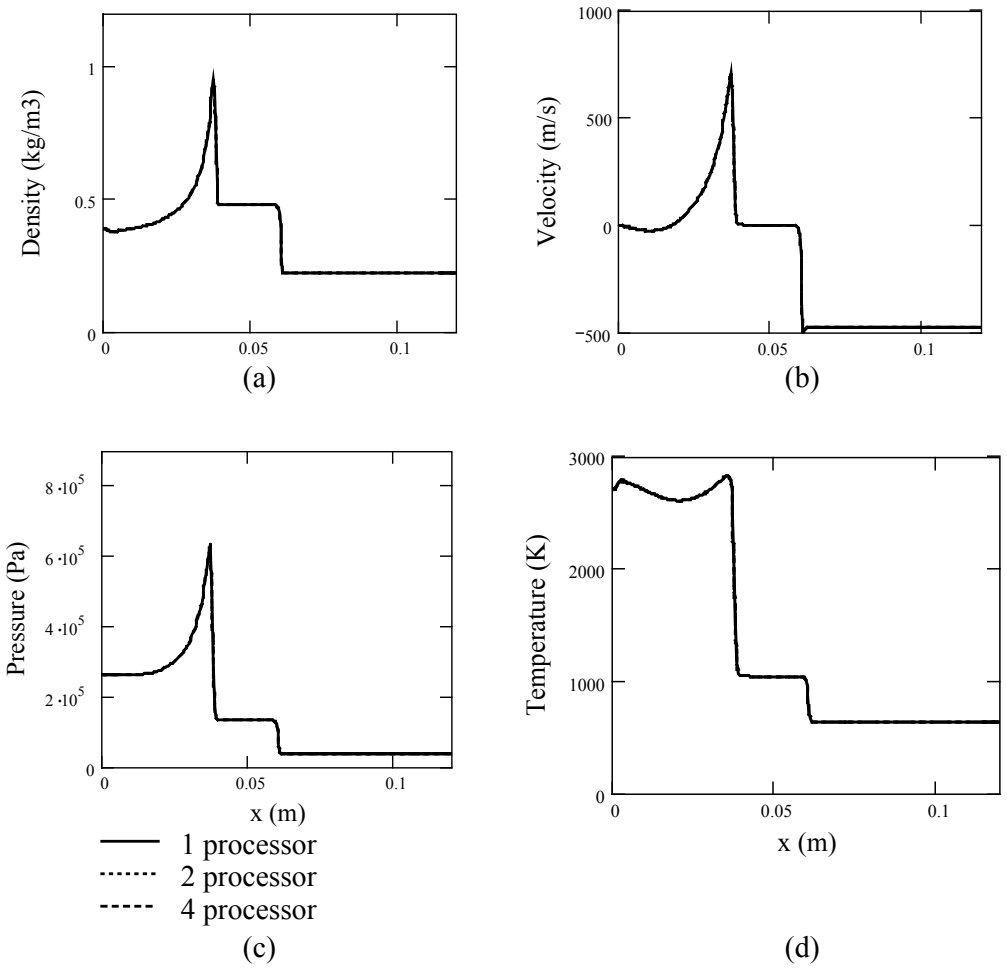

Figure 4.3 Distribution of density (a), velocity (b), pressure (c) and temperature (d) along x axis at 160 μs using single and multi processors

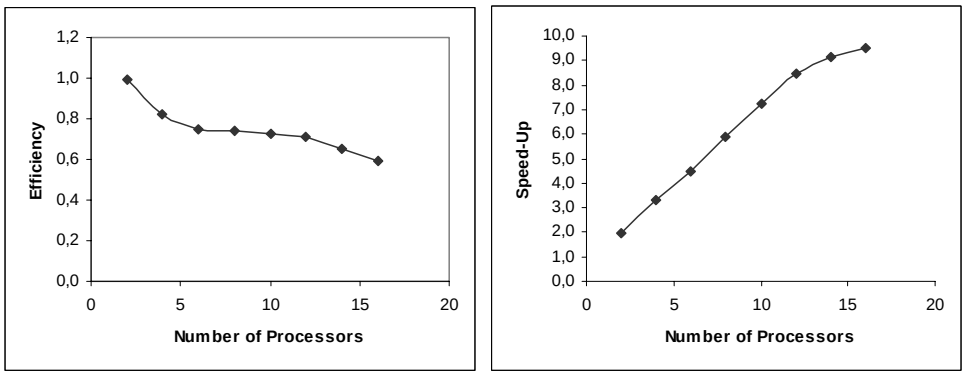

Figure 4.4 Speed-up and efficiency of parallel solver versus number of processors

Next, the grid sensitivity is studied by employing 300, 600 and 1200 cells for the solution of above problem. As shown in Figure 4.5 the solution with 600 cells provides grid independent solution. In the subsequent solutions, 600 grid cells are employed.

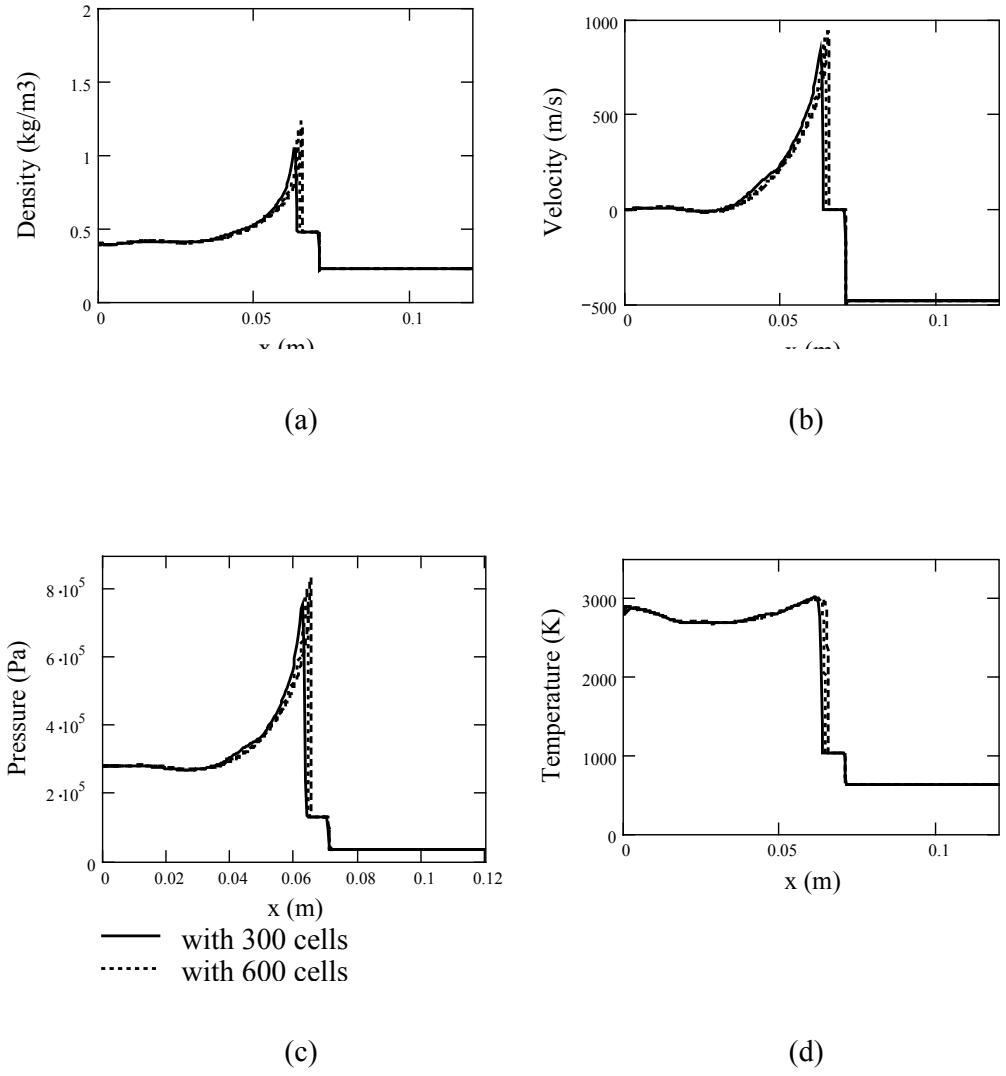

Figure 4.5 Density (a), velocity (b), pressure (c) and temperature (d) variation along x axis at 170 μs using different total mesh sizes

The time variation of the flow variables given in Figure 4.6 and Figure 4.7 shows that the chemical reactions begin at about t=100 μs and a detonation wave forms. The detonation wave travels to the right behind the reflected shock. At about t=180 μs, the detonation wave catches and overtakes the reflected shock. As the shock and detonation waves merge, some distortions and decrease are observed in Figure 4.6 and Figure 4.7. Mass fractions of all chemical species except Argon vary with time as seen in Figure 4.7, Figure 4.8 and Figure 4.9. Argon behaves as an inert gas, i.e. its concentration doesn't change in time. The amount of H_2 and O_2 decreases immediately to a negligible amount after the beginning of chemical reactions. All computations end at an instant that the detonation wave arrives to right end of the tube. It takes approximately 210 μs. Two boundary conditions are applied in the calculations; wall boundary condition at x=0 and outflow condition at x=12 cm.

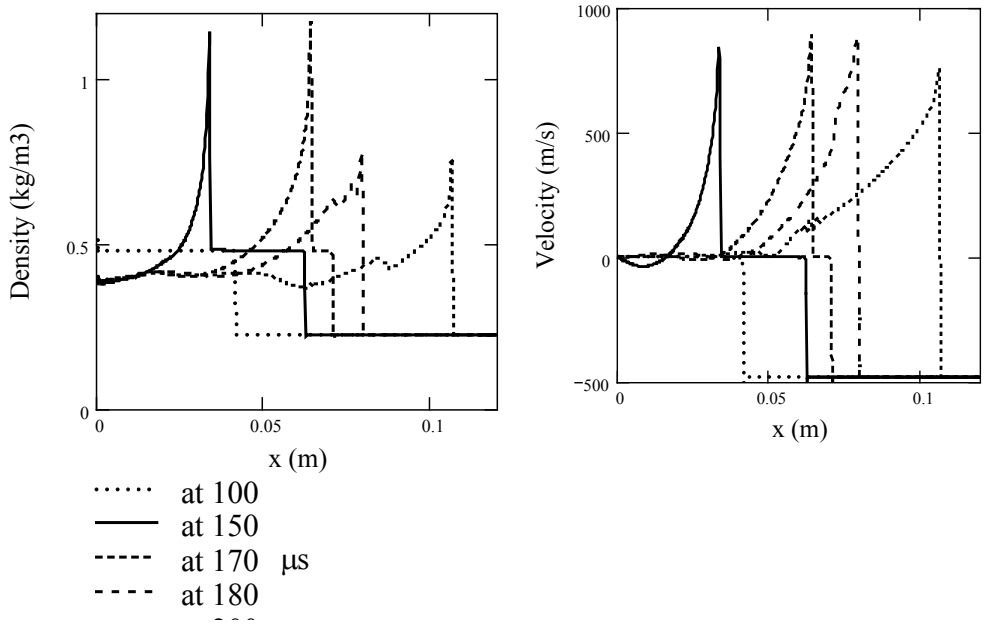

Figure 4.6 Variation of density (a) and velocity (b) in time

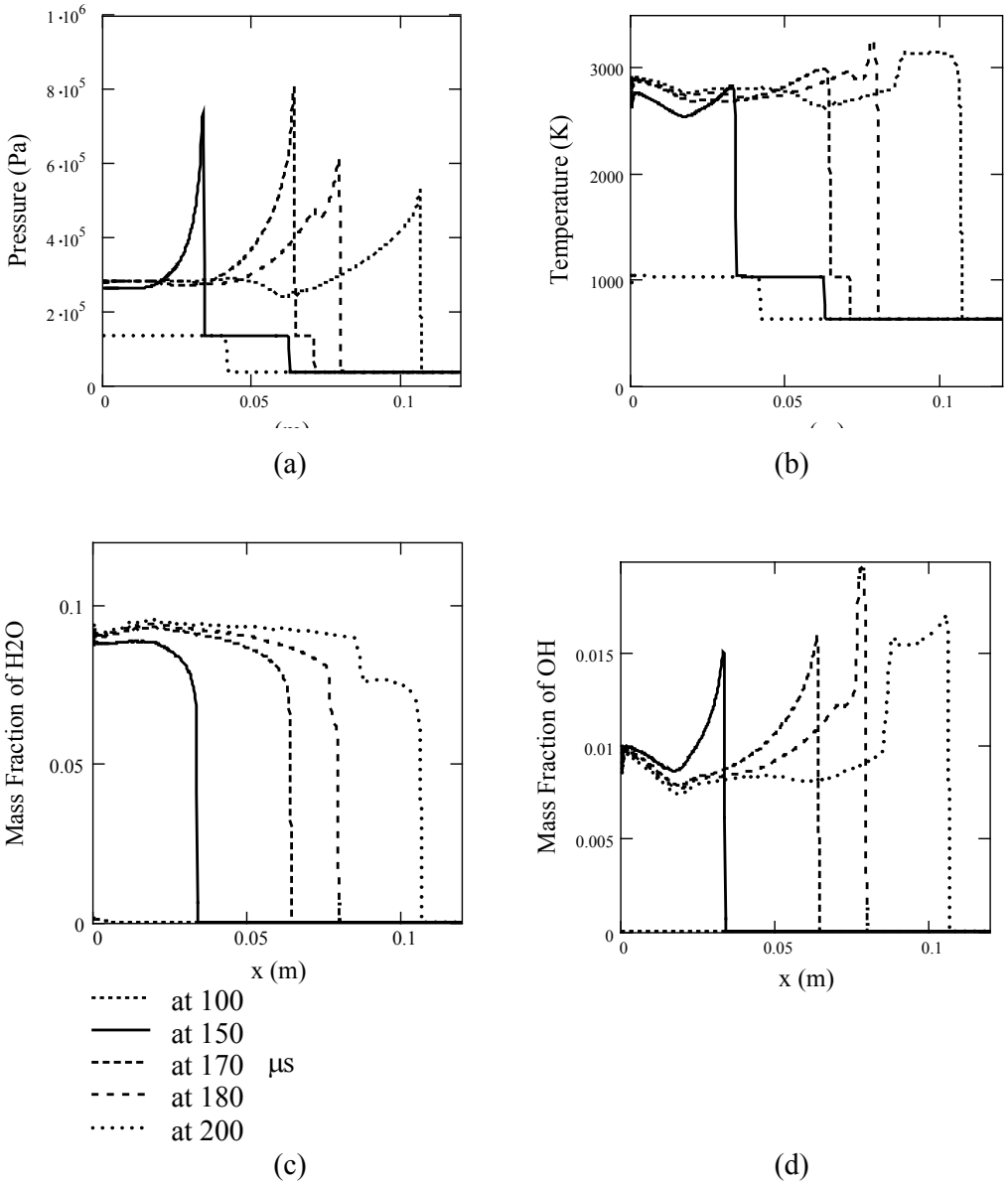

Figure 4.7 Variation of pressure (a), temperature (b) and mass fractions of H_2O (c), OH (d) in time

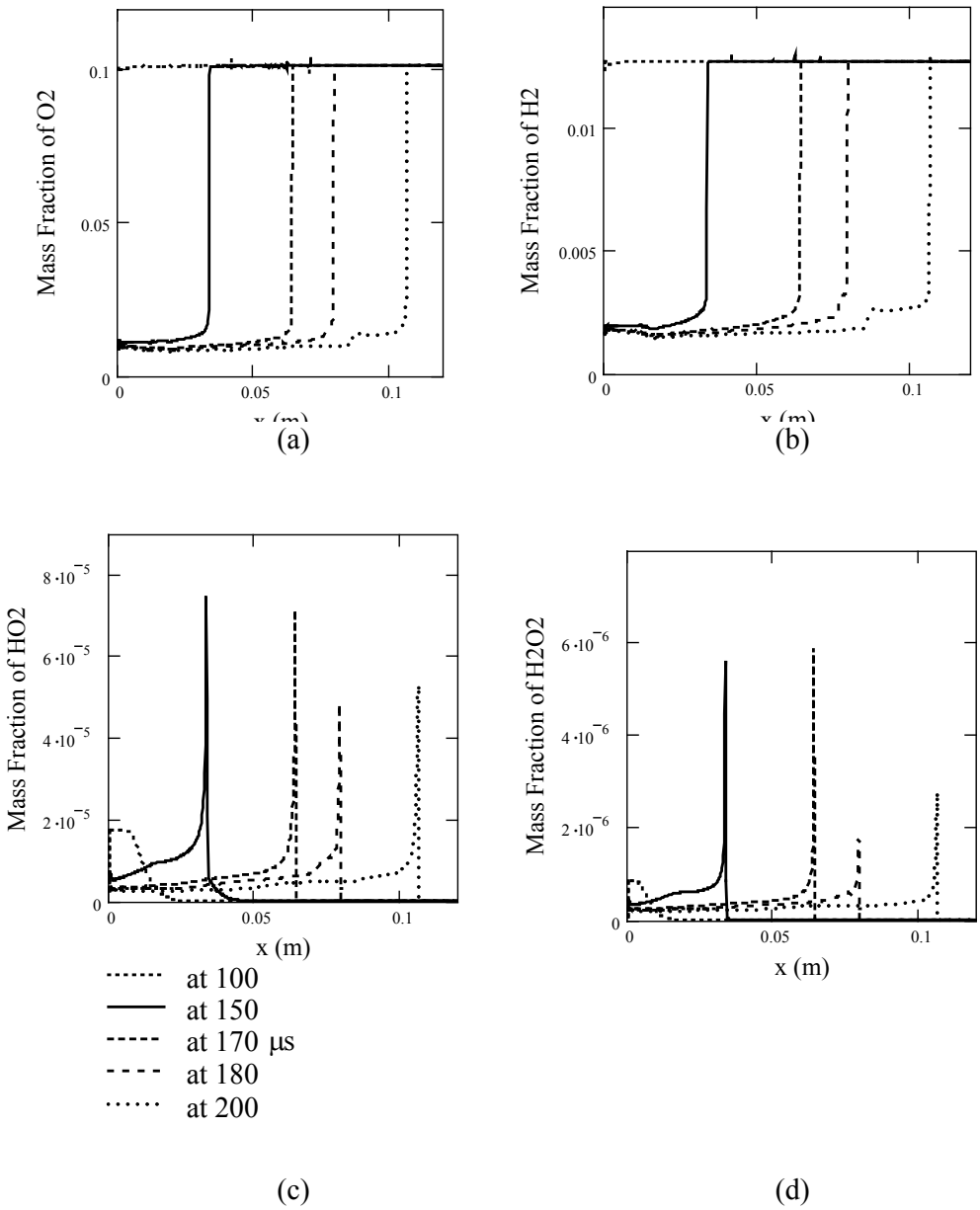

Figure 4.8 Variation of mass fractions of O_2 (a) and H_2 (b), HO_2 (c), H_2O_2 (d) in time

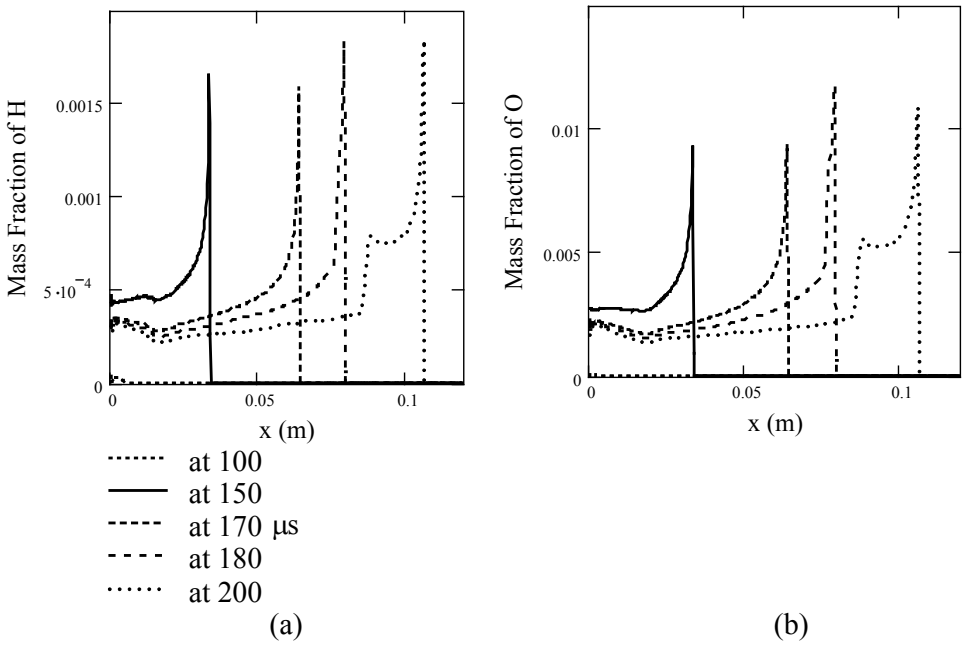

Figure 4.9 Variation of mass fractions of H (a) and O (b) in time

The present solution at t=185 μs are also compared with the data given in Reference [43] and they are shown in Figure 4.10 and Figure 4.11. In general, the solutions compare well, however there appear to be a slight shift in wave speeds, which may be attributed to the slight time difference in the extracted unsteady data.

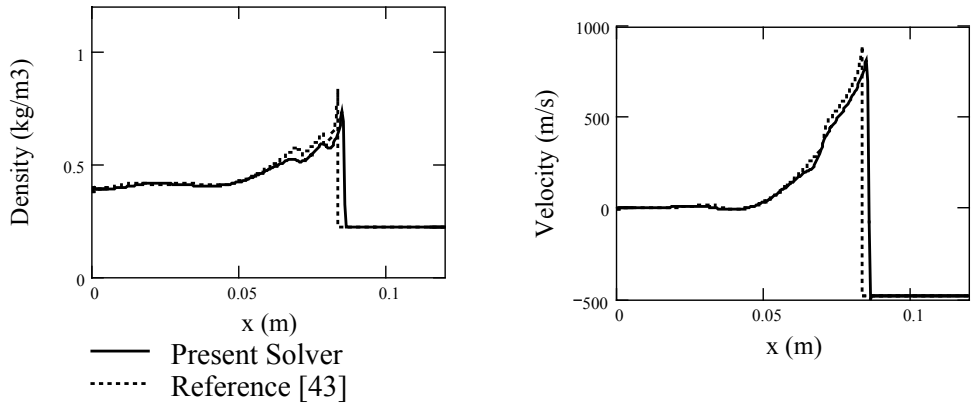

Figure 4.10 Comparison of density (a) and velocity (b) variation between present and numerical solution in Reference [43] at 185 μs

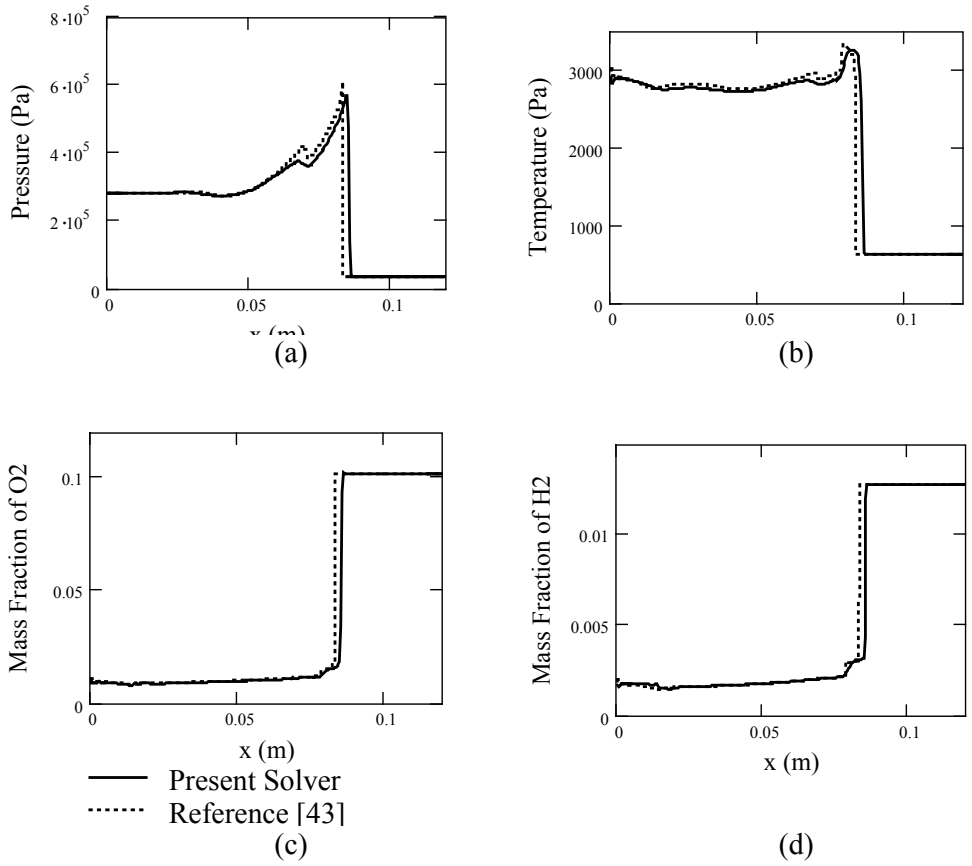

Figure 4.11 Comparison of pressure (a), temperature (b) and mass fractions of O_2(c), H_2 (d) variation between present and numerical solution in Reference [43] at 185 μs

This test case is also computed by changing the initial temperature in the tube to see its effect on the detonation formation. The solutions with T=500, 550 and 600 K at t=160 μs and t=180 μs are given in Figure 4.12 and Figure 4.13. In addition, the solutions with T=500, 550 and 600 K at t=210 μs are given in Figure 4.14. As shown for T=500 and 550 K, no significant chemical reactions are observed and detonation doesn't take place. Whereas for T=600 K chemical reactions take place immediately and the formation of a detonation wave is observed. It should be noted that as shown in Figure 4.12 (c) pressure at the wall increases due to rising in temperature. But, the negative velocities are observed in Figure 4.12 (e). These negative velocities result in a brief flow to the left.

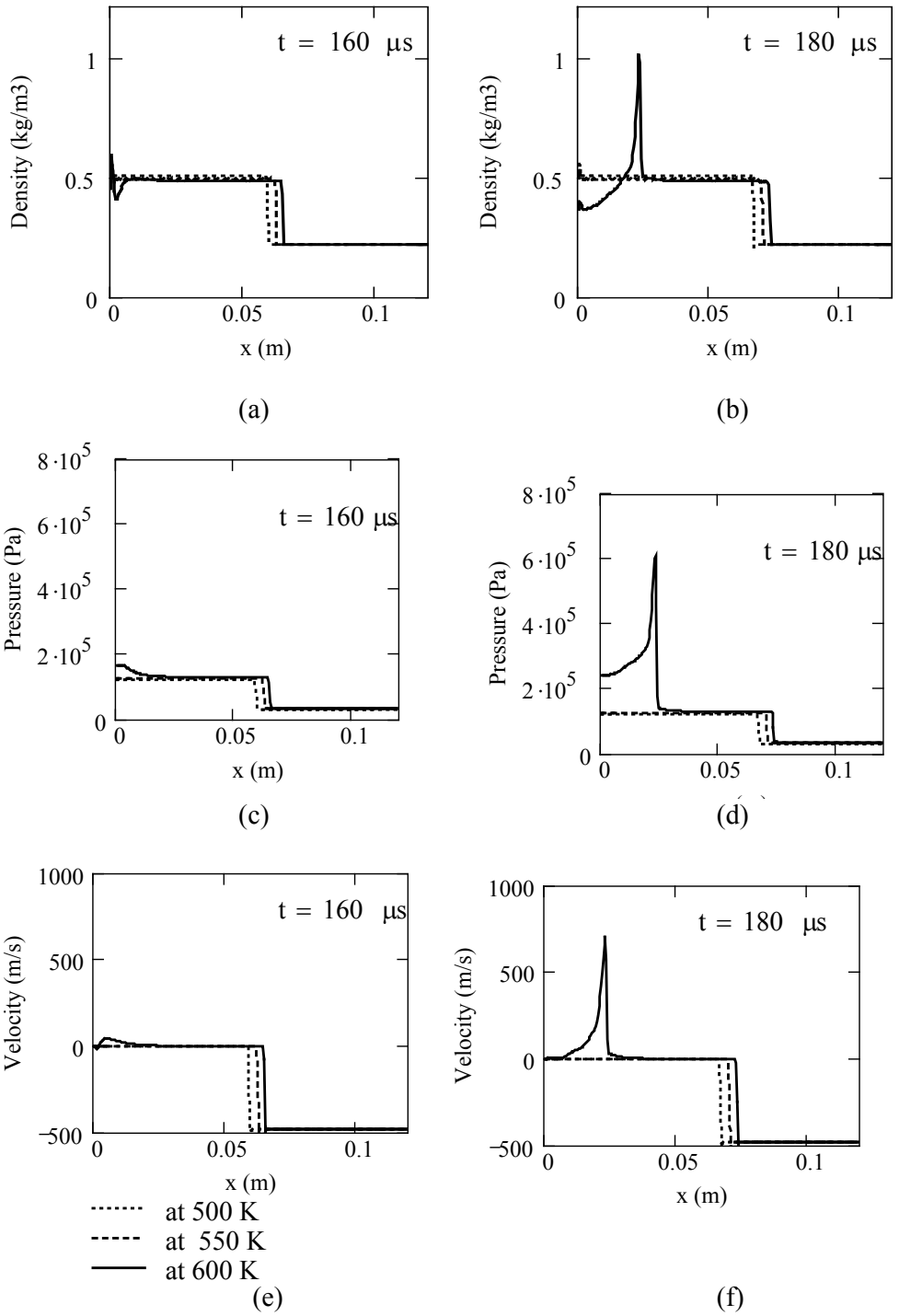

Figure 4.12 Variation of density (a,b), pressure (c,d) and velocity (e,f) at t=160 μs (a,c,e) and t=180 μs (b,d,f) for different initial temperature

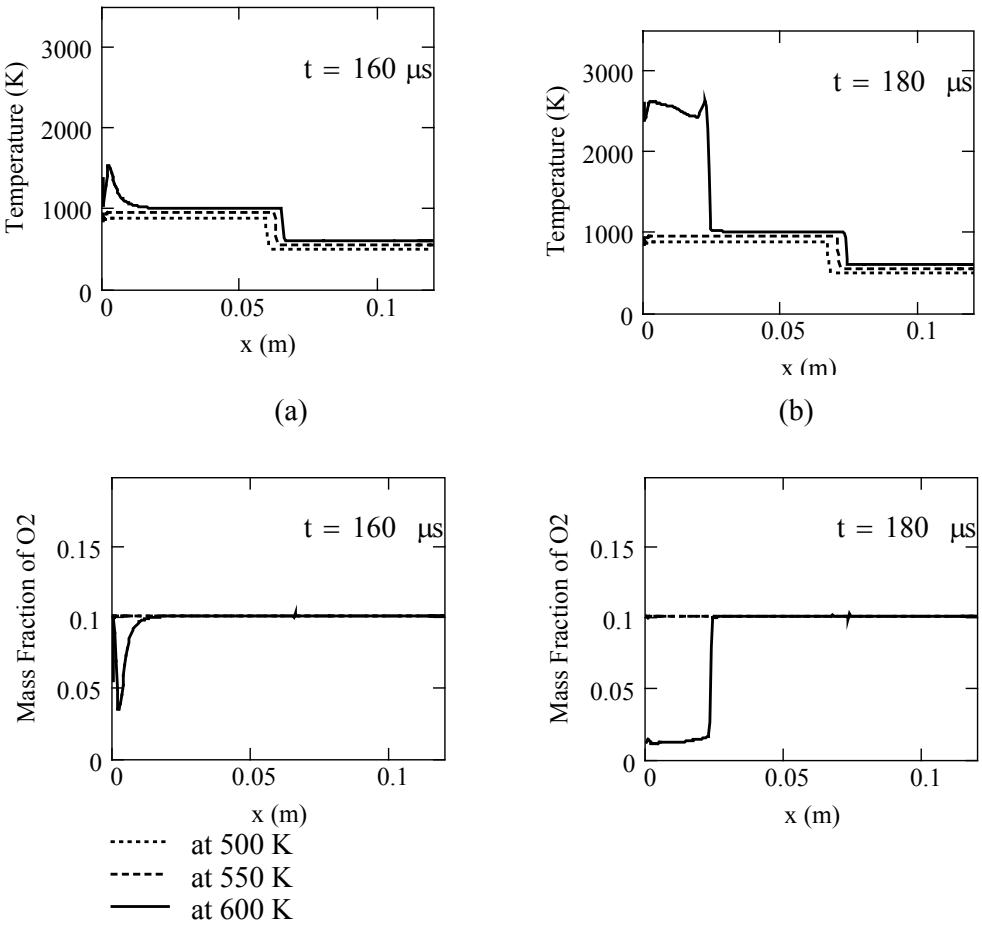

Figure 4.13 Variation of temperature (a,b) and mass fraction of O_2 (c,d) at t=160 μs (a,c) and t=180 μs (b,d) for different initial temperature

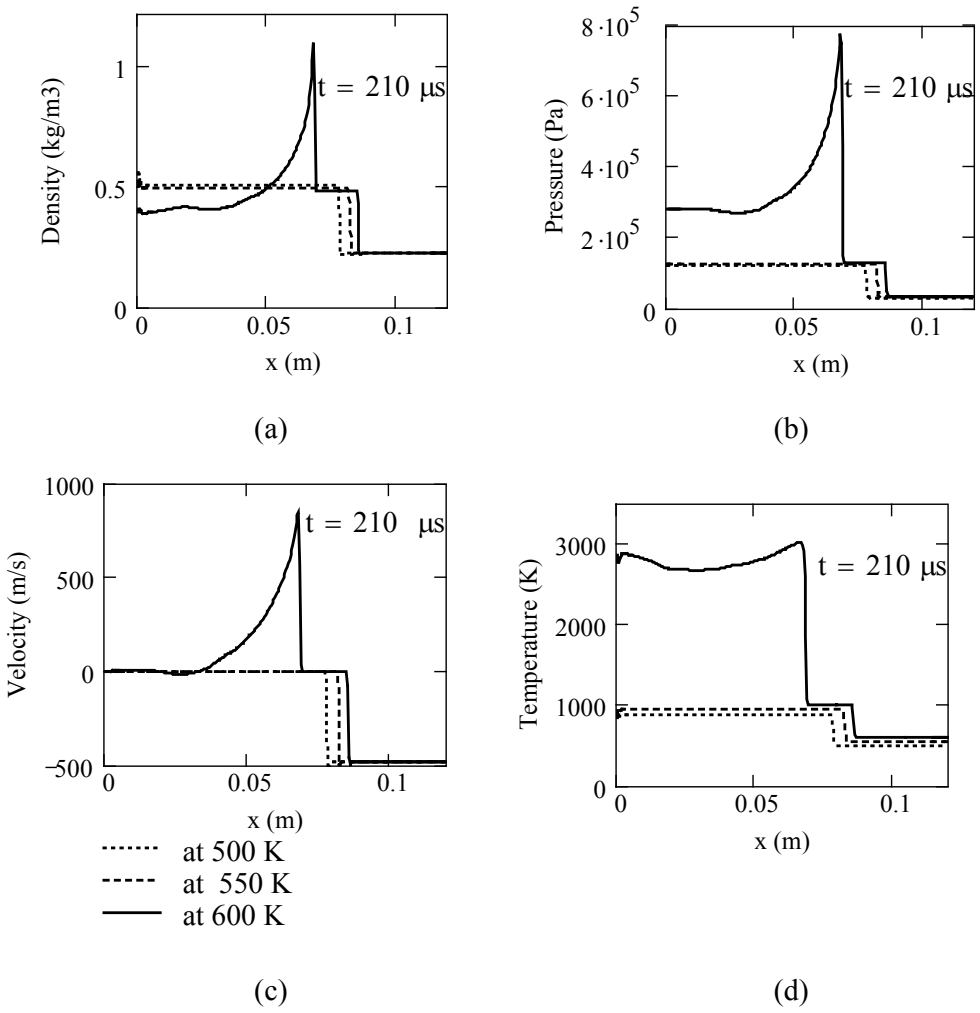

Figure 4.14 Variation of density (a), pressure (b) velocity (c) and temperature (d) at t=210 μs for different initial temperature

IV.3. Numerical Solutions with Cylindrical and Spherical Symmetry: Detonation Problem without Chemical Reactions

1D Euler Equations can be modified for 3D solutions under cylindrical or spherical symmetry conditions. As given in Eqn. (2.48), source terms are added to the governing equations.

The test case given in Reference [21] pp: 582-585 is used to validate the present solver under the cylindrical and spherical symmetry conditions. In Reference [21], cylindrical and spherical solutions are also given by a 2D solution. Solutions of two

methods are also compared in Reference [21]. The non-dimensional initial conditions are given as in Table 4.4. Symmetry boundary conditions are applied in the calculations at r=0 and r=1.The comparison of the present solution and the reference data for cylindrical and spherical symmetry are given in Figure 4.15 and Figure 4.16 respectively. As shown the present solution compares reasonably well with the reference data.

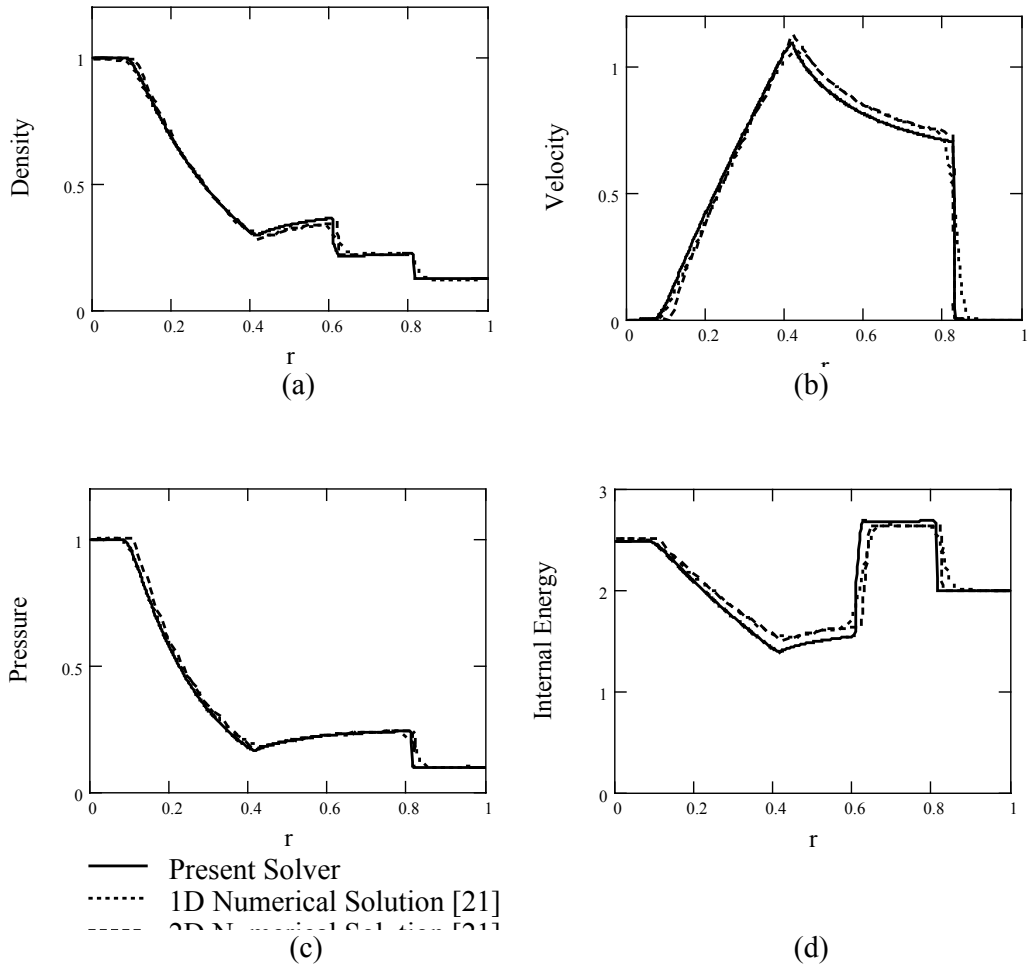

Figure 4.15 Density (a), velocity (b), pressure (c) and internal energy (d) variation along symmetry axis for cylindrical symmetry

Table 4.4 Initial Conditions for Explosion with Cylindrical and Spherical Symmetry

Variables	Inside	Outside
Pressure	1.0	0.1
Density	1.0	0.125
Velocity	0.0	0.0
Distance from Detonation	0.4	1

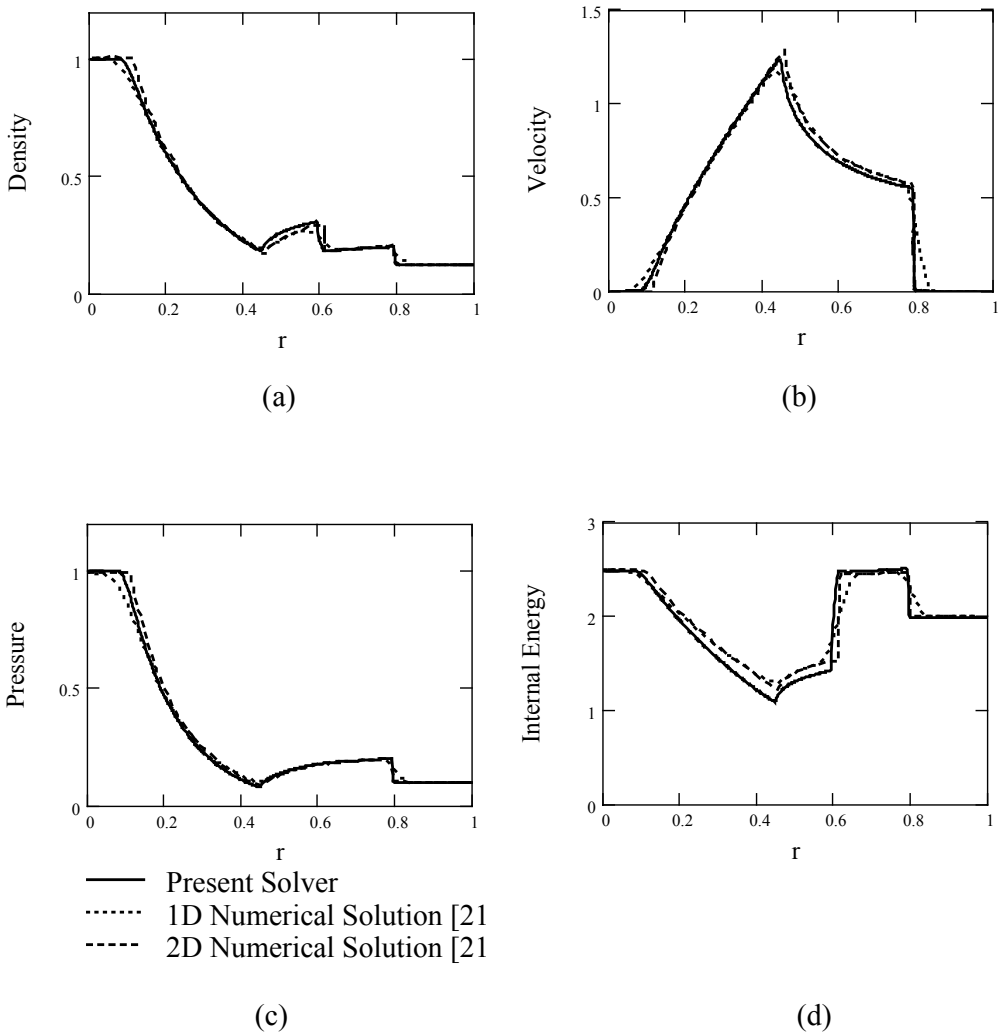

Figure 4.16 Density (a), velocity (b), pressure (c) and internal energy (d) variation along symmetry axis for spherical symmetry

IV.4. Cylindrical and Spherical Detonation of H_2:O_2:Ar with Direct Energy Deposition

Cylindrical and spherical detonation waves are next studies the present solver as a last test case. This test case is a simulation of direct initiation processes of cylindrical and spherical detonation waves by concentrated energy deposition. It should be noted that there are three initiation modes for detonation: The first one is the flame initiation, the second one is the shock wave initiation and the last one is the direct initiation mode. In all these cases, a shock wave occurs prior to detonation initiation. In the flame initiation mode, a weak spark ignites an explosive gas mixture which is confined in an enclosure. The generated flame propagates towards the unburned media. The flow motion acts as a hot-gas piston and generates a compression wave that produces a shock wave under suitable conditions. As a result, detonation occurs. In the shock initiation mode, either an incident or reflected shock wave, as in the test case 2, produce the detonation. The shock heats the unburned gas by compression. In the direct initiation mode, a large amount of energy is deposited to a small region of unconfined combustible mixture which is called as a driver section and it is shown in Figure 4.17. The rest of the region is named as a driven section. Immediately, a strong blast wave is generated. Due to shock heating, chemical reactions start and a detonation occurs under suitable conditions [44].

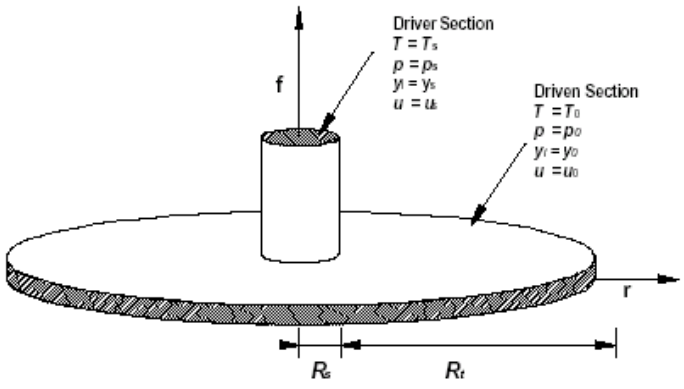

Figure 4.17 A Schematic of Initial Condition of Direct Detonation

In this validation case, direct initiation of cylindrical detonation of H_2:O_2:Ar mixture, again is modeled by using a finite-rate model of 48 reaction steps and 9 species same as in the test case 2. In reference [44], the same problem is solved using a reduced set of 24 chemical reactions and 9 species. A specific amount of energy, in the form of high pressure and temperature is deposited into driver section of a reactive gas mixture. Low temperature and pressure are set for the driven section and the initial conditions are given in as given in Table 4.5. Two boundary conditions are applied in the calculations; wall boundary condition at r=0 and outflow condition at r=0.4.

Table 4.5 Initial Data for Cylindrical and Spherical Detonation

Variables	**Driver section**	**Driven Section**
R (m)	0.008	0.4
ρ [kg/m^3]	1.2	0.223128
u [m/s]	1,000.0	0.0
P [Pa]	$2x10^6$	20,650
T [K]	3,750	298
Y_{H2}:Y_{O2}:Y_{Ar}	0.012773 : 0.101369 : 0.885858	

In Reference [44], cylindrical symmetry is used to solve a detonation wave. Mass fractions of O_2, H_2, H_2O and OH are compared with the reference data and the results are given in Figure 4.18, Figure 4.19 and Figure 4.20. In these figures, there are some jumps in the small portion of the figure near the r=0.05 m and these jumps are different for the results obtained from present solver and Reference [44]. Because, this portion is defined as a driver section and initial conditions are not given in this reference. Therefore, they are obtained from the results for test case 2. The cylindrical detonation of H_2:O_2:Ar mixture compare well with the data given in Reference [44]. As shown in Figure 4.19 and Figure 4.20, the results of present solution are better than the results of the reference data.

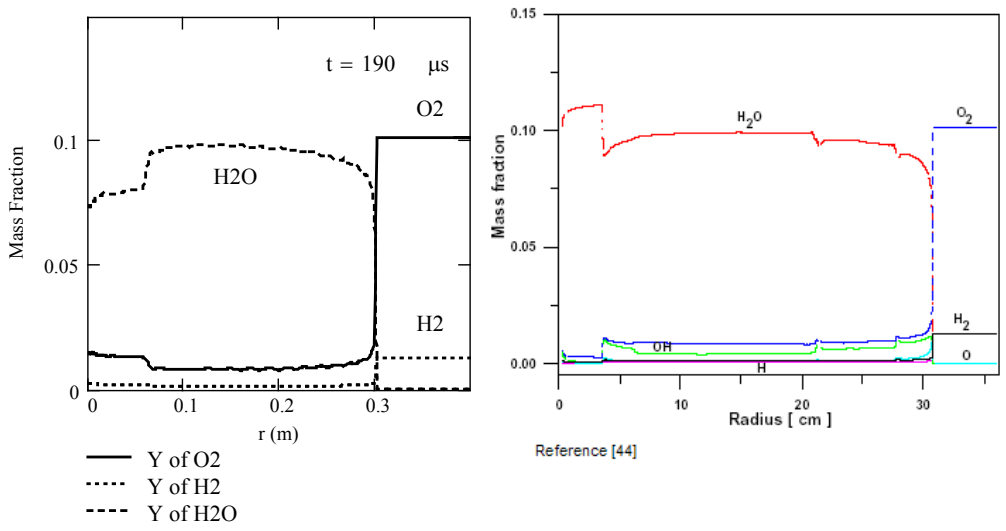

(a) (b)

Figure 4.18 Snapshot of species mass fraction for present solver (a) and Reference [44] (b) at time t=190 µs

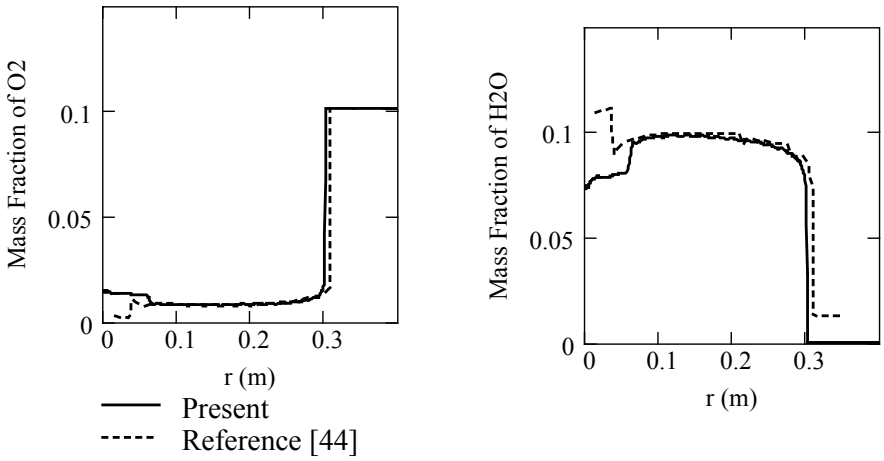

(a) (b)

Figure 4.19 Variation of Mass Fraction of O_2 (a) and H_2O (b) at time t=190 µs

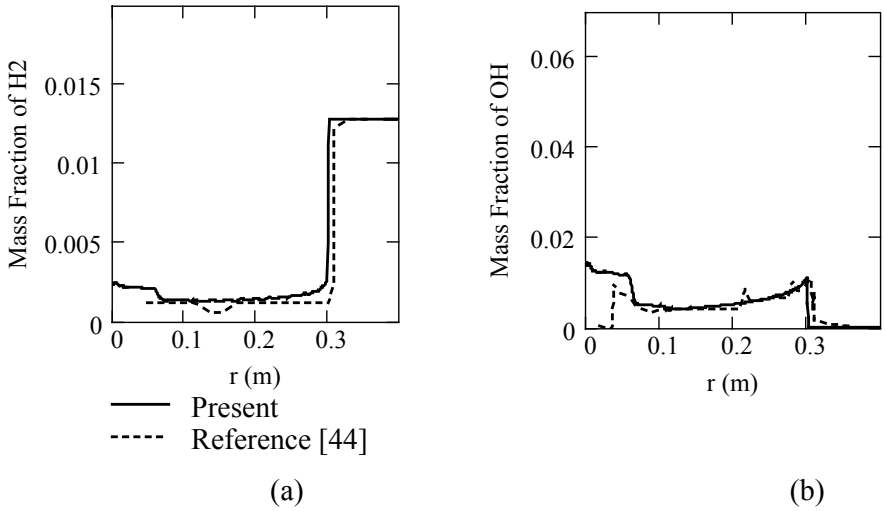

(a) (b)

Figure 4.20 Variation of Mass Fraction of H_2 (a) and OH (b) along x-axis at time t=190μs

And also, pressure variations in time are given in Figure 4.21. Peak pressure of detonation wave decreases up to t=150 μs, but it increases after this time.

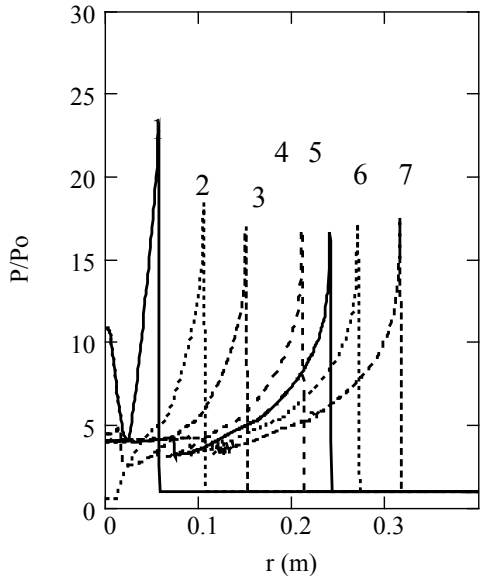

Figure 4.21 Distribution of pressure ratio along symmetry axis at (1) t=20, (2) t=50, (3) t=80, (4) t=120, (5) t=140, (6) t=160 and (7) t= 190 μs

This case is also solved under linear (when α=0) and spherical (when α=2) symmetry conditions (see Chapter II for details). The flows are computed by using the present solver at linear, cylindrical and spherical symmetry conditions. In linear case, the results are very smooth and detonation wave travels faster than the others. However, a numerical solution for cylindrical and spherical symmetry cases can only be obtained up to t=190 μs, t=80 μs respectively before they diverge (see Figure 4.22).

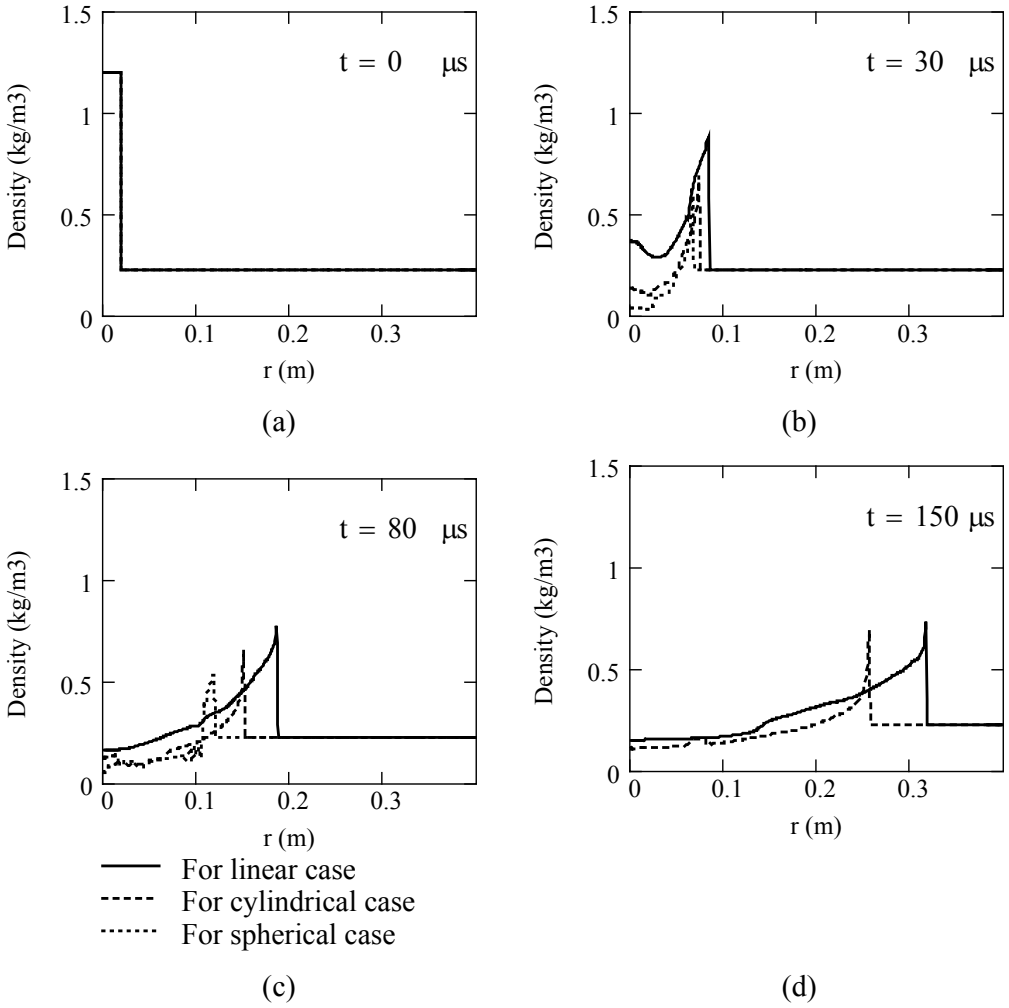

Figure 4.22 Distribution of density for linear, cylindrical and spherical detonation wave at t=0 (a), t=30 (b), t=80 (c), and t=150 μs (d)

It is seen that the spherical symmetry case is the most unstable case and since a vacuum occurs due to detonation (see Figure 4.23) and the velocity becomes negative (see Figure 4.24) which means that the flow reverses its direction abruptly and the numerical solution diverges.

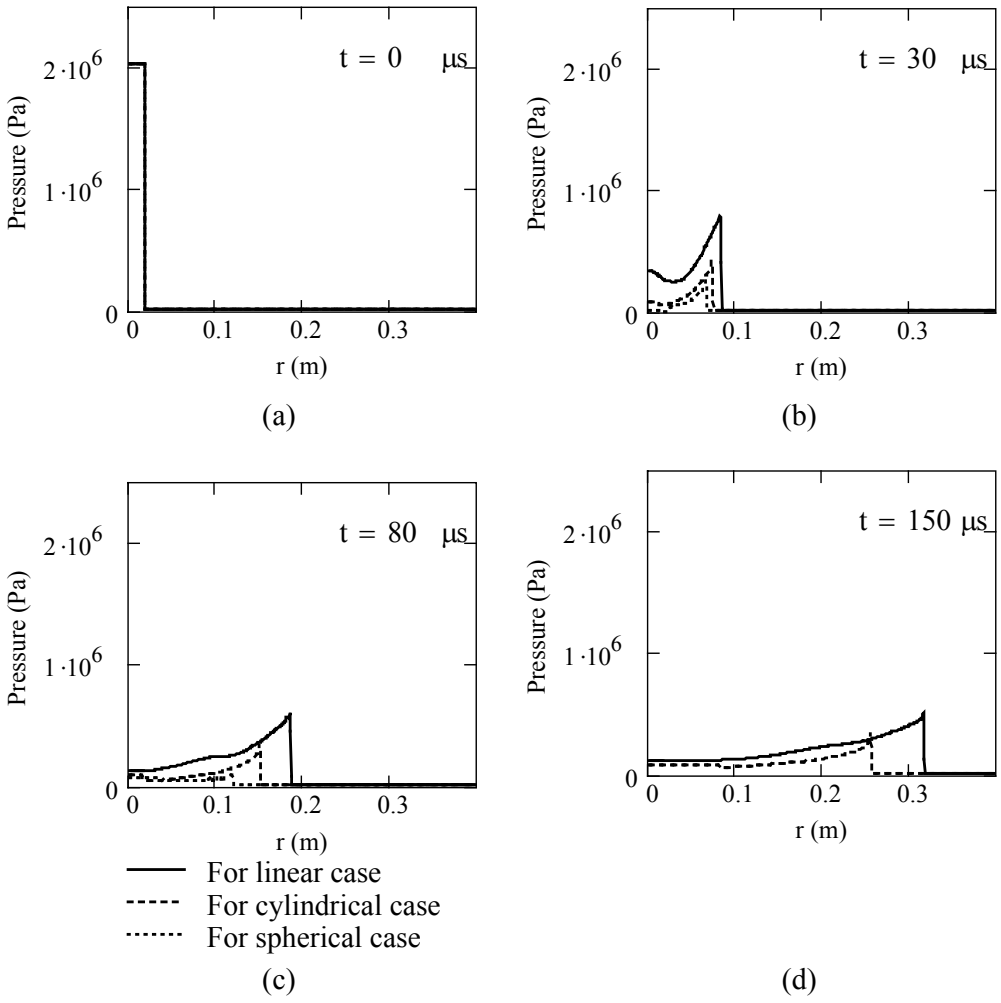

Figure 4.23 Distribution of pressure for linear, cylindrical and spherical detonation wave at t=0 (a), t=30 (b), t=80 (c), and t=150 μs (d)

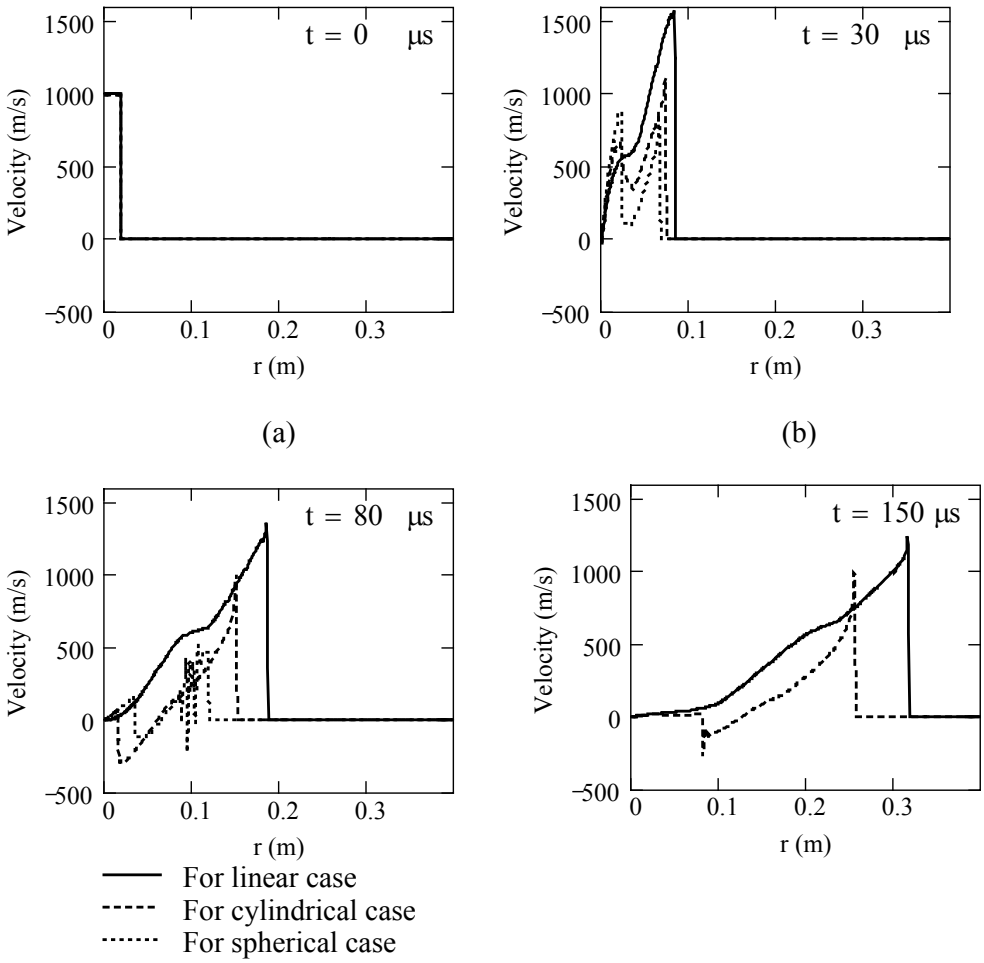

Figure 4.24 Distribution of velocity for linear, cylindrical and spherical detonation wave at t=0 (a), t=30 (b), t=80 (c), and t=150 μs (d)

It is also shown in Appendix D that the rate of change of flow variables such as density is higher in spherical symmetry case than it is in cylindrical case, which may render numerical difficulties.

The variation of mass fraction of O_2 is given lastly in Figure 4.25 and detonation front for all three cases can be seen in this figure.

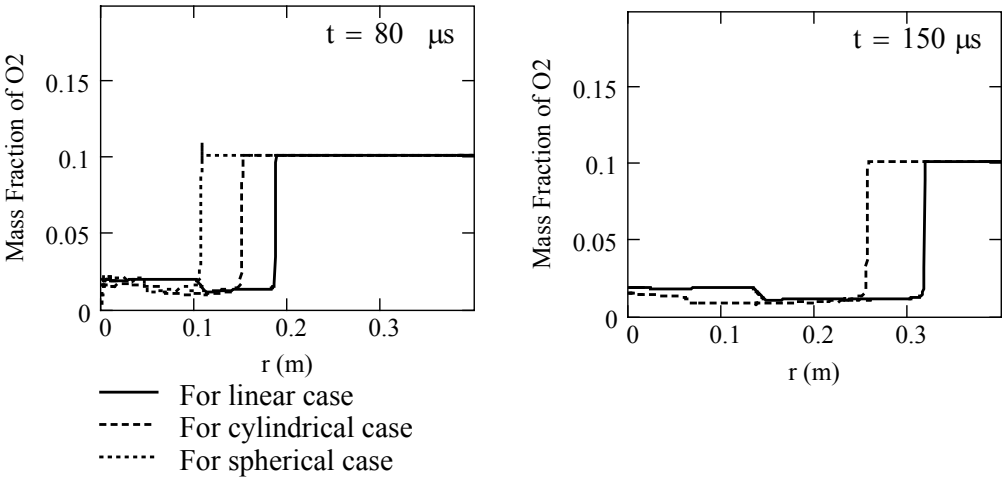

(a) (b)

Figure 4.25 Distribution of mass fraction of O_2 at t=80 (a) and t=150 μs (b)

CHAPTER V

CONCLUSIONS

In this thesis, chemically reacting flows are studied mainly for 1D detonation problems wtih the adddition of cylindrical and spherical symmetry conditions. The mathematical formulation of chemically reacting, inviscid, unsteady flows with species conservation equations and finite-rate chemistry is described. The governing equations are discretized by Finite-Volume method and solved implicitly by using a time-splitting method. Inviscid fluxes are computed using Roe Flux Difference Splitting Model. The numerical solution is implemented in parallel using domain decomposition and PVM library routines for inter-process communication.

The solution algorithm is validated first against the numerical and experimental data for a shock tube problem with chemical reactions in air and cylindrical and spherical propagation of shock wave. 1D, cylindrically and spherically symmetric detonation waves of H_2:O_2:Ar mixture are studied next. Computed results are compared with published data. The computed results and comparisons show that the developed solver is accurate, efficient and it may succesfully be employed for the solution of detonation problems such as firedamps in mines, fuel-air bombs and explosions of natural gas.

V.1. Future Work

The detonation of methane is important for both fuel-air bombs and firedamps encountered in mines. The present solver will be implemented for the detonation of methane gas in detail. The ODE solver, DLSODE, which is currently employed, will also be replaced with ROWMAP ODE solver for increasing the efficiency of the solutions.

REFERENCES

[1.] Yu S-T, *Basic Equation of Chemically Reacting Flows for Computational Fluid Dynamics*, 98-1051 AIAA/ASME/ASCE/AHS/ASC Structures, Structural Dynamics and Material Conference, 1997 (TA 645.A2), styu@me1.eng.wayne.edu

[2.] Martin, Richard T., Reza, Ali, Anderson, Larry W., *What is an explosion? A case History of an Investigation for the Insurance Indusrty*, Journal of Loss Preventation in the Process Industries, Vol.13 pp. 491-497, 2000

[3.] Kuhl, A. L, Leyer, J.-C., Borisov, A.A., Sirignano, W.A., D*ynamics of Gaseous Combustions*, AIAA Vol.151, 439 pages, 1993

[4.] Kuhl, A. L, Leyer, J.-C., Borisov, A.A., Sirignano, W.A., D*ynamic Aspects of Detonations*, AIAA Vol.153, 473 pages, 1993

[5.] Kuhl, A. L, Leyer, J.-C., Borisov, A.A., Sirignano, W.A., D*ynamic Aspects of Explosion Phenomena*, AIAA Vol.154, 563 pages, 1993

[6.] Moen, I.O., *Transition to Detonation in Fuel-Air Explosive Clouds*, Journal of Hazardous Materials, Vol. 33, pp. 159-192, 1993

[7.] Johannson, G., *Fuel Air Explosives–Revolutionise Conventional Warfare*, International Defense Review 6/1976

[8.] Technical Note 09.30/04, *Fuel-Air Explosive (FAE) Systems*, Technical Notes for Mine Action

[9.] www.hrw.org/press/2000/02/chech0215b.htm

[10.] Samirant, M., Smeets, G., Baras, C., Royer, H., and Oudin, L.R*., Dynamic Measurements in Combustible and Detonable Aerosols*, Propellants, Explosives, Pyrotechnics, Vol.14 pp. 47-56, 1989

[11.] Lavoie, L., *Fuel-Air Explosives, Weapons, and Effects*, Military Technology – MILTECH, September, 1989

[12.] Gorev, V.A., *Comparison of the Air Explosion Waves from Different Sources*, Fizika Goreniya, Vol.18, No. 1 pp. 94-101, 1982

[13.] ERDEM, Birşen, *Darbe Etkili Savaş Başlığı Raporu*, 11150.96MG01.RA.005.0, TÜBİTAK-SAGE, 1999

[14.] Fishburn, B.D., *Some Aspects of Blast from Fuel-air Explosives*, Acta Astronica, Vol.3, pp.1049-1065, 1976

[15.] Wendt, J.F., *Computational Fluid Dynamics*, Springer-Verlag, March 1996

[16.] Fletcher, C.A.J., *Computational Techniques for Fluid Dynamics*, Springer-Verlag, Volume 1 and Volume 2, 2nd Edition, 2000

[17.] Frink, N. T., Parikh P., Pirzadeh S., *A Fast Upwind Solver for the Euler Equations on Three-Dimensional Unstructured Meshes*, AIAA-91-0102

[18.] Frink, N. T., Pirzadeh S.Z., *Tetrahedral Finite-Volume Solutions to the Navier-Stokes Equations on Complex Configurations*, Internal Journal Numerical Methods in Fluids Vol.31, pp. 175-187, 1999

[19.] Hoffmann, A., K., Chiang T. S., *Computational Fluid Dynamics for Engineers*, Engineering Education System, 3rd Edition, 1993

[20.] Hirsch, C., *Numerical Computation of Internal and External Flows*, John Wiley & Sons, 1988

[21.] Toro, E.F., *Riemann Solvers and Numerical Methods for Fluid Dynamics*, Springer-Verlag, 2nd Edition, 1999

[22.] Bubsy, M. A., Cinella P., *Nonsingular Eigenvectors of the Flux Jacobian Matrix for Reactive Flows*, AIAA Journal, Vol.37, No. 3, pp. 398-401, 2000

[23.] Walters, R. W., Cinella P., Slack D. C., *Characteristic-Based Algorithms for Flows in Thermochemical Nonequilibrium*, AIAA Journal, Vol.30, No.5, pp. 1304-1313, 1992

[24.] Josyula, E., Gaitonde D., Shang J. S., *Hypersonic Nonequilibrium Flow Computations Using Roe Flux-Difference Split Sheme*, AIAA Journal, Vol.31, No.5, pp. 812-813, 1993

[25.] Mottura, L., Vigevano, L., Zaccatani, M., *An Evaluation of Roe's Scheme Generalizations for Equilibrium Real Gas Flows,* Journal of Computational Physics, Vol.138, pp. 354-399, 1997

[26.] Abgrall, R., *How to Prevent Pressure Oscillations in Multicomponent Flow Calculations: A Quasi Conservative Aproach*, Journal of Computational Physics, Vol.125, pp. 150-160, 1996

[27.] Fedkiw, R.P., Merriman, B., Osher, S., *High Accuracy Numerical Methods for Thermally Perfect Gas Flows with Chemistry*, Journal of Computational Physics, Vol.132, pp. 175-190, 1997

[28.] Chang, H.T., Hourng, L.W., Chien, L. C., *Nonequilibrium Hydrogen Combustion in One and Two Phase Supersonic Flow*, Int. Comm. Heat Mass Transfer, Vol.24, No. 3, pp. 323-335, 1997

[29.] Shuen J-S, *Upwind Differencing and LU Factorization for Chemical Nonequilibrium Navier-Stokes Equations*, Journal of Computational Physics, Vol.99, pp. 233-250, 1992

[30.] Tarhan, T., Selçuk, N., *Numerical Simulation of a Canfined Methane/Air Laminar Diffusion Flame by the Method of Lines*, Turkish Journal of Engineering Enviromental Science, Vol.27, pp.275-290, 2003

[31.] Knystautas, R. Lee, J.H.S., Shepherd, J.E., Teoderczyk, A., *Flame Acceleration and Transition to Detonation in Benzene Air Mixtures*, Combustion and Flame, Vol.115, pp. 424-436, 1998

[32.] Boni, A.A., Wilson, C.W., Chapman, M., Cook, J.L., *A study of Detonation in Methane/Air Clouds,* Acta Astronautica, Vol. 5, pp 1153-1169, 1997

[33.] Fishburn, W., *Stability of Square-Wave Detonation in a Model System*, Physica, Vol.16, pp.358-370, 1985

[34.] Hall, F.S., Ludford, G.S.S., *Stability of a Detonation Wave*, Physica, Vol. 28, pp.1-17, 1987

[35.] Zhou, X., Brenner G., Weber, T., Durst, F., *Finite-Rate Chemistry in Modelling of Two-dimensional Jet Premixed CH_4/air Flame,* International Journal of Heat and Mass Transfer, Vol.42, pp. 1757-1773, 1999

[36.] Umeda, J., Fujivana, J., *Methane Combustion in Multi-Stratified Vortical Flow Field*, Energy Convers. Mgmt. Vol.38, No. 10-13, pp. 1101-1110, 1997

[37.] Fotache, C.G., Wang, H., Law, C.K., *Ignition of Ethan, Propane and Butane in Counterflow Jets of Cold Fuel Versus Hot Air under Variable Pressures*, Combustion and Flame, Vol.117, pp. 777- 794, 1999

[38.] Ak, M., A., *Analysis of Transient Regimes in Solid Rocket Propulsion*, Ph.D. Distertion, Department of Mechanical Engineering, Middle East Technical University, 2001

[39.] Kuo, K.K., *Principles of Combustion*, John Wiley and Sons Inc., 1986

[40.] Turns, S., R., A*n Introduction to Combustion*, McGraw Hill, 2nd Edition, 2000

[41.] Luke, E., A., *A Rule-Based Specification System for Computational Fluid Dynamics*, Ph.D. Distertion, Department of Computational Engineering, Mississippi State, 1999

[42.] Keyes, D., Ecer, A., Periaux, J., Satofuka, N., *Parallel Computational Fluid Dynamics Towards Teraflops*, North Holland, 1st Edition, 2000

[43.] www-ian.math.uni-magdeburg.de Grambow, Dr. W., Magdeburg University, Faculty of Mathematics, 39106 Magdeburg, Germany

[44.] Im, K.-S., Yu, S.-T., J. *Analyses of Direct Detonation Initiation with Realistic Finite-Rate Chemistry,* MI48202, Mechanical Engineering Department of Wayne State University, Detroit

APPENDIX A

NON-CONSERVATIVE FORM OF EULER EQUATIONS WITH FINITE RATE CHEMISTRY

Conservative form of Euler Equations with finite rate chemistry is:

$$\frac{\partial Q}{\partial t} + \frac{\partial E}{\partial x} = S$$

where

$$Q = \begin{bmatrix} \rho u \\ \rho E \\ \rho_1 \\ \rho_2 \\ . \\ . \\ \rho_{N_s} \end{bmatrix} \qquad E = \begin{bmatrix} \rho u^2 + P \\ u(\rho E + P) \\ u\ \rho_1 \\ u\rho_2 \\ . \\ . \\ u\rho_{N_s} \end{bmatrix} \qquad \mathrm{S} = \begin{bmatrix} 0 \\ 0 \\ \dot{w}_1 \\ \dot{w}_2 \\ . \\ . \\ \dot{w}_{N_s} \end{bmatrix} \tag{A.1}$$

Conservation of mass of the gas mixture;

$$\frac{\partial \rho}{\partial t} + \frac{\partial (\rho u)}{\partial x} = 0$$
$$\frac{\partial \rho}{\partial t} + u\frac{\partial \rho}{\partial x} + \rho\frac{\partial u}{\partial x} = 0 \tag{A.2}$$

From (A.1), conservation of momentum is as follows;

$$\frac{\partial (\rho u)}{\partial t} + \frac{\partial (\rho u^2 + p)}{\partial x} = 0 \tag{A.3}$$

Then, it can be different form as:

$$\rho\frac{\partial u}{\partial t} + u\frac{\partial \rho}{\partial t} + u^2\frac{\partial \rho}{\partial x} + 2u\rho\frac{\partial u}{\partial x} + \frac{\partial p}{\partial x} = 0 \tag{A.4}$$

Take the paranthesis,

$$u\left(\frac{\partial \rho}{\partial t}+u\frac{\partial \rho}{\partial x}+\rho\frac{\partial u}{\partial x}\right)+\rho\left(\frac{\partial u}{\partial t}+u\frac{\partial u}{\partial x}+\frac{1}{\rho}\frac{\partial p}{\partial x}\right)=0 \tag{A.5}$$

Using (A.2) we get (A.4) as below;

$$\frac{\partial u}{\partial t}+u\frac{\partial u}{\partial x}+\frac{1}{\rho}\frac{\partial p}{\partial x}=0 \tag{A.6}$$

Similarly, if we rewrite the enegy equation in (A.1),

$$\frac{\partial \rho E}{\partial t}+\frac{\partial u(\rho E+p)}{\partial x}=0 \tag{A.7}$$

and the total energy E of the gas mixture is defined as;

$$E = e + \frac{u^2}{2} \tag{A.8}$$

Then, it can be different form as:

$$\begin{aligned}&\rho\frac{\partial e}{\partial t}+u\rho\frac{\partial u}{\partial t}+e\frac{\partial \rho}{\partial t}+\frac{u^2}{2}\frac{\partial \rho}{\partial t}+\rho e\frac{\partial u}{\partial x}+\rho\frac{u^2}{2}\frac{\partial u}{\partial x}+\\&p\frac{\partial u}{\partial x}+ue\frac{\partial \rho}{\partial x}+\frac{u^3}{2}\frac{\partial \rho}{\partial x}+u\rho\frac{\partial e}{\partial x}+u^2\rho\frac{\partial u}{\partial x}+u\frac{\partial p}{\partial x}=0\end{aligned} \tag{A.9}$$

Take the e, $u^2/2$, $u\rho$ and ρ paranthesis, we get

$$\begin{aligned}&e\left(\frac{\partial \rho}{\partial t}+\rho\frac{\partial u}{\partial x}+u\frac{\partial \rho}{\partial x}\right)\\&+\frac{u^2}{2}\left(\frac{\partial \rho}{\partial t}+\rho\frac{\partial u}{\partial x}+u\frac{\partial \rho}{\partial x}\right)\\&+u\rho\left(\frac{\partial u}{\partial t}+u\frac{\partial u}{\partial x}+\frac{1}{\rho}\frac{\partial p}{\partial x}\right)\\&+\rho\left(\frac{\partial e}{\partial t}+u\frac{\partial e}{\partial x}+\frac{p}{\rho}\frac{\partial u}{\partial x}\right)=0\end{aligned} \tag{A.10}$$

The first and second terms of Eqn. (A.10) is the conservation of mass and the third terms of Eqn. (A.10) is the conservation of momentum equation. Hence, the conservation of energy can be written in terms of primitive variables

$$\frac{\partial e}{\partial t}+u\frac{\partial e}{\partial x}+\frac{p}{\rho}\frac{\partial u}{\partial x}=0 \tag{A.11}$$

If we write the conservation of mass for species *i*, then it is seen that the non-conservative form of

$$\frac{\partial \rho_i}{\partial t} + \frac{\partial (\rho_i u)}{\partial x} = \dot{\omega}_i \qquad i = 1,2,...,N_s$$
$$\frac{\partial \rho_i}{\partial t} + u\frac{\partial \rho_i}{\partial x} + \rho_i \frac{\partial u}{\partial x} = \dot{\omega}_i \tag{A.12}$$

As a result, the non-conservative form of equation has obtained from the conservative form of equations

$$\frac{\partial u}{\partial t} + u\frac{\partial u}{\partial x} + \frac{1}{\rho}\frac{\partial p}{\partial x} = 0$$
$$\frac{\partial e}{\partial t} + u\frac{\partial e}{\partial x} + \frac{p}{\rho}\frac{\partial u}{\partial x} = 0$$
$$\frac{\partial \rho_1}{\partial t} + u\frac{\partial \rho_1}{\partial x} + \rho_1 \frac{\partial u}{\partial x} = \dot{\omega}_1 \tag{A.13}$$
$$\frac{\partial \rho_2}{\partial t} + u\frac{\partial \rho_2}{\partial x} + \rho_2 \frac{\partial u}{\partial x} = \dot{\omega}_2$$
...
$$\frac{\partial \rho_{N_s}}{\partial t} + u\frac{\partial \rho_{N_s}}{\partial x} + \rho_{N_s} \frac{\partial u}{\partial x} = \dot{\omega}_{N_s}$$

APPENDIX B

DERIVATION OF p_e AND $p_{\rho i}$

(See Reference [1])

Assume the ideal gas equation for the gas mixture,

$$p = T\sum_{i=1}^{N_s} \rho_i R_i = \rho RT \tag{B.1}$$

Thus, the change of p can be expressed as

$$dp = \left(\frac{\partial p}{\partial T}\right)_{\rho_j} dT + \sum_{i=1}^{Ns}\left(\frac{\partial p}{\partial \rho_i}\right)_{T,\rho_{j,j\neq i}} d\rho_i \tag{B.2}$$

Accordingt to Eqn. (B.1), the partial derivatives of p can be expressed as

$$\begin{aligned}\left(\frac{\partial p}{\partial T}\right)_{\rho_j} &= \sum_{i=1}^{N_s} \rho_i R_i = \rho R \\ \left(\frac{\partial p}{\partial \rho_i}\right)_{T,\rho_{j,j\neq i}} &= R_i T\end{aligned} \tag{B.3}$$

Then insert the above partial derivatives into (B.2)

$$dp = \rho R dT + R_i T d\rho_i \tag{B.4}$$

So, p_e can be found by using (B.4),

$$\begin{aligned}p_e &= \rho R\left(\frac{\partial T}{\partial e}\right)_{\rho_j} + R_i T\left(\frac{\partial \rho_i}{\partial e}\right)_{\rho_{j,j\neq i}} \\ &= \rho R\left(\frac{\partial T}{\partial e}\right)_{\rho_j} = \frac{\rho R}{C_v} = (\gamma - 1)\rho\end{aligned} \tag{B.5}$$

Similarly, $p_{\rho i}$ can be obtained,

$$p_{\rho_i} = \rho R\left(\frac{\partial T}{\partial \rho_i}\right)_{e,\rho_{j,j\neq i}} + \sum_{k=1}^{Ns} R_k T\left(\frac{\partial \rho_k}{\partial \rho_i}\right)_{T,\rho_{j,j\neq i}}$$
$$= \rho R\left(\frac{\partial T}{\partial \rho_i}\right)_{e,\rho_{j,j\neq i}} + R_i T \tag{B.6}$$

To find below terms in Eqn. (B.6), use internal energy relation,

$$\left(\frac{\partial T}{\partial \rho_i}\right)_{e,\rho_{i,j\neq i}}$$

$$e = \sum_{i=1}^{Ns} \frac{\rho_i}{\rho}\left(\int_{Tref}^{T} C_{p_i} dT + h_{f_i}\right) - \frac{T}{\rho_i}\sum_{i=1}^{Ns} \rho_i R_i \tag{B.7}$$

$$0 = de = \left(\frac{\partial e}{\partial T}\right)_{\rho_j} dT + \sum_{i=1}^{Ns}\left(\frac{\partial e}{\partial \rho_i}\right)_{T,\rho_{j,j\neq i}} d\rho_i$$
$$= C_v dT + \sum_{i=1}^{Ns}\left(\frac{e_i - e}{\rho}\right) d\rho_i \tag{B.8}$$

where *e=const*

$$\left(\frac{\partial T}{\partial \rho_i}\right)_{e,\rho_{i,j\neq i}} = \frac{(e_i - e)}{\rho C_v} \tag{B.9}$$

Substitute (B.8) into (B.6), we get,

$$p_{\rho_i} = \frac{R}{C_v}(e_i - e) + R_i T \tag{B.10}$$

Finally, substitude (B.5) and (B.10) into (B.2)

$$dp = \frac{\rho R}{C_v} de + \sum_{i=1}^{Ns}\left[\frac{R}{C_v}(e_i - e) + R_i T\right] d\rho_i \tag{B.11}$$

APPENDIX C

LEFT EIGENVECTOR MATRICES OF NON-CONSERVATIVE AND CONSERVATIVE FORM OF EQUATIONS

The matrix N^{-1} is the left eigenvector matrix of the non-conservative equations.

$$N^{-1} = \frac{1}{\gamma p}\begin{bmatrix} \gamma p/2 & a p_e/2 & a p_{\rho_1}/2 & a p_{\rho_2}/2 & a p_{\rho_{Ns}}/2 \\ \gamma p/2 & -a p_e/2 & -a p_{\rho_1}/2 & -a p_{\rho_2}/2 & -a p_{\rho_{Ns}}/2 \\ 0 & \rho_1 p_{\rho_1} & -p_{\rho_1}\left(\gamma p - \rho_1 p_{\rho_1}\right)/p_e & \rho_1 p_{\rho_1} p_{\rho_2}/p_e & \rho_1 p_{\rho_1} p_{\rho_{Ns}}/p_e \\ 0 & \rho_2 p_{\rho_2} & \rho_2 p_{\rho_2} p_{\rho_1}/p_e & -p_{\rho_2}\left(\gamma p - \rho_2 p_{\rho_2}\right)/p_e & \rho_2 p_{\rho_2} p_{\rho_{Ns}}/p_e \\ \cdots & \cdots & \cdots & \cdots & \cdots \\ 0 & \rho_{Ns} p_{\rho_{Ns}} & \rho_{Ns} p_{\rho_{Ns}} p_{\rho_1}/p_e & \rho_{Ns} p_{\rho_{Ns}} p_{\rho_2}/p_e & -p_{\rho_{Ns}}\left(\gamma p - \rho_{Ns} p_{\rho_{Ns}}\right)/p_e \end{bmatrix} \quad \text{(C.1)}$$

The matrix K^{-1} is the left eigenvector matrix of the conservative equations.

$$K^{-1} = \begin{bmatrix} (\gamma p - a p_e u)/2 & a p_e/2 & \left(-\gamma p u + a p_e\left(u^2 - E\right) + a\rho p_{\rho_1}\right)/2 & \left(-\gamma p u + a p_e\left(u^2 - E\right) + a\rho p_{\rho_2}\right)/2 & \dots & \left(-\gamma p u + a p_e\left(u^2 - E\right) + a\rho p_{\rho_{Ns}}\right)/2 \\ (\gamma p + a p_e u)/2 & -a p_e/2 & \left(\gamma p u + a p_e\left(u^2 - E\right) + a\rho p_{\rho_1}\right)/2 & \left(-\gamma p u - a p_e\left(u^2 - E\right) - a\rho p_{\rho_2}\right)/2 & \dots & \left(-\gamma p u - a p_e\left(u^2 - E\right) - a\rho p_{\rho_{Ns}}\right)/2 \\ -\rho_1 p_{\rho_1} u & \rho_1 p_{\rho_1} & \rho_1 p_{\rho_1}\left(u^2 - E + \rho p_{\rho_1}/p_e\right) - \rho\hat{h} p_{\rho_1} & \rho_1 p_{\rho_1}\left(u^2 - E + \rho p_{\rho_2}/p_e\right) & \dots & \rho_1 p_{\rho_1}\left(u^2 - E + \rho p_{\rho_{Ns}}/p_e\right) \\ -\rho_2 p_{\rho_2} u & \rho_2 p_{\rho_2} & \rho_2 p_{\rho_2}\left(u^2 - E + \rho p_{\rho_1}/p_e\right) & \rho_2 p_{\rho_2}\left(u^2 - E + \rho p_{\rho_2}/p_e\right) - \rho\hat{h} p_{\rho_2} & \dots & \rho_2 p_{\rho_2}\left(u^2 - E + \rho p_{\rho_{Ns}}/p_e\right) \\ \dots & \dots & \dots & \dots & \dots & \dots \\ -\rho_{Ns} p_{\rho_{Ns}} u & \rho_{Ns} p_{\rho_{Ns}} & \rho_{Ns} p_{\rho_{Ns}}\left(u^2 - E + \rho p_{\rho_1}/p_e\right) & \rho_{Ns} p_{\rho_{Ns}}\left(u^2 - E + \rho p_{\rho_2}/p_e\right) & \dots & \rho_{Ns} p_{\rho_{Ns}}\left(u^2 - E + \rho p_{\rho_{Ns}}/p_e\right) - \rho\hat{h} p_{\rho_{Ns}} \end{bmatrix} \quad \text{(C.2)}$$

APPENDIX D

TIME RATE OF CHANGE OF DENSITY FOR CYLINDRICAL AND SPHERICAL CASE

The continuity equation can be written as follows:

$$\frac{d}{dt}\int_{\forall}\rho d_{\forall} = -\int_{A}\rho\vec{u}\cdot\vec{d}_{A} \tag{D.1}$$

As take the density and velocity are constants along the area and volume, Eqn. (D.1) can be written as follows:

$$\frac{d}{dt}(\rho)\forall = -\rho u A \tag{D.2}$$

For cylinder, area and volume can be defined as;

$$\begin{aligned} A_c &= 2\pi r\lambda \\ \forall_c &= \pi r^2\lambda \end{aligned} \tag{D.3}$$

For sphere, area and volume can be defined as;

$$\begin{aligned} A_s &= 4\pi r^2 \\ \forall_s &= \frac{4}{3}\pi r^3 \end{aligned} \tag{D.4}$$

When Eqn's. (D.3) and (D.4) are substituted into Eqn. (D.2), time rate of change can be written under the cylindrical and spherical conditions as follows.

$$\left.\begin{aligned} \frac{d}{dt}(\rho)_s &= -\frac{3\rho u}{r} \\ \frac{d}{dt}(\rho)_c &= -\frac{2\rho u}{r} \end{aligned}\right\} \Rightarrow \frac{\frac{d}{dt}(\rho)_s}{\frac{d}{dt}(\rho)_c} = \frac{3}{2} \tag{D.5}$$

As a result, the rate of change of flow variables such as density is higher in spherical symmetry case than it is in cylindrical case.